Research Article

Resubmission

MDM2 integrates cellular respiration and apoptotic signaling through NDUFS1 and the mitochondrial network.

Rana Elkholi[1,3,4], Ioana Abraham-Enachescu[1,3], Andrew P. Trotta[1,3], Camila Rubio-Patiño[1,3], Jarvier N. Mohammed[1,3], Mark P. A. Luna-Vargas[1,3], Jesse D. Gelles[1,3,4], Joshua R. Kaminetsky[1,2], Madhavika N. Serasinghe[1,2,3], Cindy Zou[6], Sumaira Ali[6], Gavin P. McStay[6,§], Cathie M. Pfleger[1,3,4], and Jerry Edward Chipuk[1,2,3,4,5,*]

[1] Department of Oncological Sciences,

[2] Department of Dermatology,

[3] The Tisch Cancer Institute,

[4] The Graduate School of Biomedical Sciences,

[5] The Diabetes, Obesity, and Metabolism Institute,

Icahn School of Medicine at Mount Sinai, One Gustave L. Levy Place, New York, New York 10029 USA

[6] Department of Life Sciences, New York Institute of Technology, Northern Boulevard, Old Westbury, New York, 11568 USA

[§] Current Affiliation: Department of Biological Sciences, Staffordshire University, Stoke-on-Trent, Staffordshire, UK

[*] To whom correspondence should be addressed: Jerry Edward Chipuk, Ph.D., Department of Oncological Sciences, Icahn School of Medicine at Mount Sinai, 1425 Madison Avenue, Box 1130, New York, New York 10029 USA, Telephone: +1 (212) 659-5543; Facsimile: +1 (212) 987-2240; jerry.chipuk@mssm.edu

KEYWORDS

Apoptosis, BCL-2 Family, Complex I, MDM2, Mitochondria, NDUFS1

SUMMARY

Signaling diversity and subsequent complexity in higher eukaryotes is partially explained by one gene encoding a polypeptide with multiple biochemical functions in different cellular contexts. For example, mouse double minute 2 (MDM2) is functionally characterized as both an oncogene and tumor suppressor, yet this dual classification confounds the cell biology and clinical literatures. Identified via complementary biochemical, organellar, and cellular approaches, we report that MDM2 negatively regulates NADH:ubiquinone oxidoreductase 75 kDa Fe-S protein 1 (NDUFS1), leading to decreased mitochondrial respiration, marked oxidative stress, and commitment to the mitochondrial pathway of apoptosis. MDM2 directly binds and sequesters NDUFS1 preventing its mitochondrial localization, ultimately causing Complex I and supercomplex destabilization, and inefficiency of oxidative phosphorylation. The amino terminal region of MDM2 is sufficient to bind NDUFS1, alter supercomplex assembly, and induce apoptosis. Finally, this pathway is independent of p53, and several mitochondrial phenotypes are observed in *Drosophila* and murine models expressing transgenic *Mdm2*.

INTRODUCTION

Using two distinct promoters and twelve exons, the *Mdm2* gene produces a host of mRNA transcripts leading to the expression of full-length wild-type MDM2 and multiple disease-related isoforms (Fakharzadeh et al., 1991; Momand et al., 1992; Iwakuma and Lozano 2003; Vousden and Prives 2005; Singh et al., 2009; Jeyaraj et al., 2009). The wild-type 90-kDa MDM2 protein contains motifs that are essential for its function, including: nuclear localization and nuclear export signals (NLS and NES), a central core consisting of an acidic region and a zinc finger domain, and a carboxyl terminus RING finger, which is responsible for an E3 ubiquitin ligase activity (Tan et al., 2017). Together, these attributes define a complex network of subcellular localizations, diverse binding partners, and post-translational modifications that affect and effect MDM2 signaling (Manfredi, 2010).

Early studies on MDM2 highlighted the fundamental observation that MDM2 levels in human tumor samples range from 5 – 50 fold over basal expression suggesting an oncogenic role by blocking p53 function (Oliner et al., 1992; Bueso-Ramos et al., 1993; Bueso-Ramos et al., 1995; Bueso-Ramos et al., 1996). In contrast, a tumor suppressor activity was revealed in primary tissues as transgenic *Mdm2* mice expressing just two fold over physiological levels were challenging to generate (Jones et al., 1998). Curiously, transgenic *Mdm2* mice demonstrate dose-dependent susceptibility to tumor burden: animals expressing two copies of the *Mdm2* transgene have shorter tumor-free survival compared to a single copy of the transgene, and the tumor spectrum greatly differs from *trp53*$^{-/-}$ mice (Jones et al., 1998). *In situ* functional dissection between MDM2 and p53 is also suggested by the observation that human tumors can harbor both MDM2 over-expression and mutant p53. A short time after MDM2 was described to have an oncogenic function, several studies revealed that MDM2 over-expression correlated with poor patient prognosis in multiple cancer types (Reifenberger et al., 1993; Matsumura et al., 1996). However, few studies provide mechanistic insights into how MDM2 signaling disrupts cellular homeostasis beyond direct links to DNA metabolism and the p53 pathway (Saadatzadeh et al., 2017). Here, we show that cytosolic MDM2 binds and sequesters a component of Complex I, NDUFS1 (NADH:ubiquinone oxidoreductase 75 kDa Fe-S protein 1), which leads to a loss in mitochondrial bioenergetics, marked reactive oxygen species generation, and in several cellular models, commitment to the mitochondrial pathway of apoptosis.

RESULTS

MDM2 regulates cellular survival independent of its canonical functions. Based on the above literature, we hypothesized that MDM2 may promote signaling that is either incompatible with homeostasis (*i.e.,* tumor suppressor function) --- and/or facilitates cellular transformation (*i.e.,* oncogenic function) --- by selecting for apoptosis-incompetent cells. To examine this hypothesis in the absence of confounding p53-mediated effects, we evaluated ectopic MDM2 expression in a functionally-null p53 deficient human non-small cell lung cancer cell line, H1299. First, H1299 were transiently transfected with increasing amounts of *Mdm2* cDNA, and this led to dose-dependent cell death within 48 hours (Fig. 1A). MDM2 has two well-defined features: (1) it functions in association with its binding partner, MDMX; and (2) a robust E3 ubiquitin ligase activity (Tan et al., 2017). Therefore, we tested if either were required for MDM2-induced cell death. To do so, the *MDMX* gene was stably silenced using three shRNAs in H1299, and then these cells were transfected with MDM2 cDNA. Silencing of *MDMX* did not produce any significant changes in cell death responses compared to the scrambled RNAi control (Figs. 1B, S1A); and co-expression of MDM2 and MDMX did not alter the extent or rate of cell death (Figs. S1B-F). Furthermore, ectopic expression of a catalytic cysteine mutant (C464A; Kubbutat et al., 1999) of MDM2 that fails to function as an E3 ubiquitin ligase also induced potent, dose-dependent cell death responses (Figs. 1C, S1G). To determine if ectopically expressed MDM2 functioned as expected within the canonical p53 pathway, we also compared MDM2's effects in the presence of ectopic p53. H1299 were transfected with *TRP53* cDNA, which resulted in marked cell death; and co-expression of p53 and MDM2 or MDM2 C464A (binds p53 but cannot degrade) prevented the cell death responses, suggesting that transiently expressed MDM2 was functional (Figs. 1D, S1G-H).

To expand these cell death observations into additional p53 null contexts, we transiently transfected MDM2 into HCT116$^{TRP53-/-}$, A549 with stable expression of *TRP53* RNAi, and mouse embryonic fibroblasts (MEFs) with recombined floxed *Trp53* alleles; and these cell lines also demonstrated dose-dependent cell death when MDM2 was expressed (Fig. 1E). We corroborated these results by examining a MDM2 mutant (MDM2^{G58A}; Freedman et al., 1997) that fails to bind p53, and its expression also led to cell death comparable to MDM2^{WT} (Fig. 1F). Based on the data in 1D, we reasoned that the p53·MDM2 complex could negatively regulate

MDM2-induced cell death, and disruption may reveal cell death responses. To examine this possibility, we compared two human non-small cell lung cancer lines: H460 and H23, which express $p53^{WT}$ or a structural mutant of p53 that fails to bind DNA and induce pro-apoptotic transcriptional responses ($p53^{R246I}$), respectively. These cell lines were transiently transfected with MDM2, and then treated with Nutlin-3A, a small molecule that disrupts the p53·MDM2 complex (Vassilev et al., 2004). While $MDM2^{WT}$ expression or Nutlin-3A treatment alone did not influence cell survival in the presence of endogenous p53, the combination promoted equivalent cell death in both lines further suggesting the cellular response to MDM2 was not likely mediated by p53-dependent transcription (Fig. 1G). Finally, the above studies focused on transient expression of MDM2, and therefore we were interested in extending these investigations by using a doxycycline-inducible MDM2 system. H1299 with stable $MDM2^{TetOn}$ were treated with doxycycline, and assayed for cell death. Similar to our results with transient models (Figs. 1A-G), induction of MDM2 protein led to time-dependent cell death that peaked around 48 hours (Figs. 1H-I). These observations suggest that MDM2 promotes cell death independent of its well-described functions.

MDM2-induced cell death is engaged by the mitochondrial pathway of apoptosis. As murine (MDM2) and human MDM2 (HDM2) proteins are 80% conserved, we determined if they produced comparable cell death results. Indeed, H1299 expressing either MDM2 or HDM2 resulted in marked cell death (Fig. 2A), and subsequent cell death assays, we primarily focused on MDM2, but corroborated the key findings using HDM2 (data not shown). Multiple mechanisms control cell death, and we next defined the signaling pathway required for MDM2-induced death. First, we examined the morphology of DAPI-stained nuclei from cells that died following MDM2 expression, and marked nuclear fragmentation was apparent suggesting apoptosis as the mechanism of death (Fig. 2B). To determine if this was correct, we performed kinetic cell death analysis using live-cell high-content imaging of H1299 expressing MDM2 in the presence of zVAD-fmk, an irreversible inhibitor to the apoptotic caspases. While MDM2 induced dose- and time-dependent death, nearly all of this death was blocked by zVAD-fmk (Figs. 2C-D). Cells marked as dead in these assays led to a loss of clonogenic survival (Fig. 2E), and death was not prevented by the co-expression of a dominant negative FADD (which inhibits

death receptor induced apoptosis; Fig. 2F), suggesting the mitochondrial pathway of apoptosis is induced by MDM2.

The BCL-2 family is the key mediator of the mitochondrial pathway of apoptosis by regulating mitochondrial outer membrane permeabilization (MOMP), caspase activation, and irreversible commitment to death (Chipuk et al., 2010). We screened whole cell lysates from H1299 expressing MDM2 for changes to BAK, BAX, and BIM, which are the BCL-2 family effectors and a BH3-only protein that collaborate to engage the majority of stress-induced apoptosis; but no gross changes were apparent (Fig. 2G); and mRNA changes were also not observed (data not shown). As BIM is the critical BH3-only protein that functions at mitochondria to activate BAK/BAX leading to apoptosis, we next determined if BIM was localized to mitochondria following MDM2 expression. H1299 cells were transfected with MDM2 in the presence of zVAD-fmk to prevent death, whole cell and mitochondrial extracts were isolated, and analyzed by SDS-PAGE and western blot for BIM. MDM2 caused the accumulation of the short isoform of BIM (BIM-S) within the mitochondrial fraction (Fig. 2H); and RNAi-mediated silencing of *BIM* maintained survival of MDM2-expressing cells (Figs. 2I, S2A). The pro-apoptotic function of BIM is to activate BAX and/or BAK; therefore, we tested if knockdown of *BAX* or *BAK* also promoted survival. Indeed, RNAi mediated silencing of *BAX* or *BAK* resulted in rescue from MDM2-induced death (Figs. 2J, S2B, S2D-G); and this paralleled activation-induced conformational changes in BAX (Fig. S2C), while silencing other BH3-only proteins (*e.g.,* BID & PUMA) did not alter MDM2-induced death (Figs. S2D-G). Next, we examined the impact of anti-apoptotic BCL-2 (*e.g.,* BCL-xL, MCL-1) proteins to regulate MDM2-induced death. H1299 expressing MDM2 alone, or in the presence of BCL-xL or MCL-1, were analyzed for cell death. Co-expression of BCL-xL or MCL-1 inhibited cell death responses (Fig. 2K); and a complementary loss of function experiment with ABT-737, a small molecule BH3 mimetic that inhibits multiple anti-apoptotic BCL-2 proteins resulted in enhanced death (Oltersdorf et al., 2005; Fig. 2L). Together, these data suggest that the mitochondrial pathway of apoptosis mediates MDM2-induced death.

To explore the greater impact of MDM2-induced apoptosis in cell biology, we utilized *Drosophila melanogaster* expressing *MDM2* under control of the *GAL4/UAS* system, which allows for tissue-specific expression, and is temperature sensitive to allow increased expression at higher temperatures (Folberg-Blum et al., 2002). We chose *Drosophila* because they have

conserved stress signaling and cell death pathways; yet, the *Drosophila* p53 pathway is not regulated by mammalian MDM2, and there is no *Drosophila* MDM2 homolog to confound interpretations. As shown in figure 2M, *Drosophila* expressing MDM2 in the eye (*GMR>MDM2)* at 21°C demonstrate cellular stress revealed by smaller, rough, less organized eye tissue that is dependent upon gene dosage; and temperature-dependent increased expression of MDM2 led to dose-dependent tissue ablation (Figs. S2H-I). When *GMR>MDM2* animals were crossed against strains that genetically disable cellular commitment to apoptosis (*H99*, a deletion that eliminates *reaper/grim/hid* to prevent the initiation of apoptotic signaling; transgenic *DIAP1* or *p35*, suppress caspase activation; Davidson et al., 1998; White et al., 1994), the majority of MDM2-induced eye phenoytpes were suppressed (Fig. 2N). Similar results were also obtained using a wing-specific promoter (Fig. S2J). Moreover, 96.8% of *GMR>MDM2* flies reared at 30°C failed to eclose suggesting marked developmental abberations, but when crossed into apoptosis-deficient backgrounds, flies successfully eclosed at rates approaching Mendelian ratios (Fig. 2O). These results suggested that MDM2-induced stress and subsequent apoptotic responses are observable in numerous cell types and tissues.

The MDM2 amino terminal domain (amino acids 1-101) is sufficient to promote the mitochondrial pathway of apoptosis and causes genomic and oxidative stress. MDM2 has several functional domains, and we examined which was required for MDM2-induced apoptosis (Fig. 3A). H1299 were transfected with the indicated truncated versions of MDM2, and scored for apoptosis. $MDM2^{1-227}$ was the most potent mediator of cell death (Fig. 3B), its expression level was similar to the other MDM2 variants (Fig. 3C), and the observed death was regulated by zVAD-fmk, ABT-737, and BCL-xL as predicted suggesting $MDM2^{1-227}$ also induced the mitochondrial pathway of apoptosis (Figs. 3D-E). Moreover, we generated further deletions of MDM2 (data not shown), and narrowed down a minimal amino terminal 101 amino acid region ($MDM2^{1-101}$) that was a potent-inducer of dose-dependent apoptosis (Fig. 3F).

To better understand MDM2 initiated stress and subsequent apoptosis, we explored how MDM2 localization impacted on cell death. First, we determined $MDM2^{WT}$ and $MDM2^{1-101}$ localization by immunofluorescence, as they both are potent inducers of apoptosis. Ectopic expression of these untagged proteins was detected throughout the cell, with relatively similar nuclear and cytosolic distributions (Fig. 3G). As such, we then compared how mutation of the

nuclear localization signal (NLS-) and nuclear export signal (NES-) influenced apoptosis induced by full-length MDM2. These mutant forms of MDM2 resulted in expected cellular localizations: $MDM2^{NLS-}$ and $MDM2^{NES-}$ were cytosolic and nuclear, respectively (Fig. 3H); and their expression levels by western blot were similar to $MDM2^{WT}$ (Fig. 3I). Interestingly, $MDM2^{WT}$ and $MDM2^{NLS-}$ demonstrated equivalent dose-dependent apoptotic responses (Fig. 3J); $MDM2^{NES-}$ produced no apoptotic responses alone or when combined with ABT-737 (data not shown) --- and these data suggested that MDM2 stress signaling originates from the cytoplasm.

We screened through several macromolecular stress pathways (*e.g.,* unfolded protein response, oxidative damage, and DNA damage) and noted that H1299 cells expressing $MDM2^{WT}$ or $MDM2^{1-101}$ demonstrated marked nuclear γH2AX accumulation (Fig. 3K) and $Chk1^{Ser345}$ phosphorylation (Fig. 3L), two markers of DNA damage and downstream double strand break signaling. In addition, we analyzed metaphase spreads, and noted that both $MDM2^{WT}$ and $MDM2^{1-101}$ expression produced severe genomic damage as evidenced by chromosome and chromatid breaks (Fig. 3M). Continued screening also revealed that $MDM2^{WT}$ and $MDM2^{1-101}$ expression also resulted in marked cellular ROS production (Fig. 3N), which upon further examination, was likely mitochondrial in origin as ROS was detected by a mitochondrial-specific probe (MitoSOX, Fig. 3O). In experiments not shown, we could not detect activation of the unfolded protein response. These observations served as the basis that MDM2 expression results in mitochondrial ROS production, DNA damage, and subsequent apoptosis.

MDM2 binds NDUFS1 to destabilize supercomplex-assembled Complex I and promote ROS. As mitochondrial ROS is produced by the electron transport chain (ETC), we examined how MDM2 influenced mitochondrial respiration. H1299 expressing either $MDM2^{WT}$, $MDM2^{NLS-}$, or $MDM2^{1-101}$ were subjected to Seahorse MitoStress analysis, and these MDM2 variants which demonstrate cytosolic accumulation also reduced basal and maximal oxygen consumption rates (OCR; Figs. 3G-H, 4A, S3A); whereas cells expressing $MDM2^{NES-}$, which is restricted to the nucleus (Fig. 3H), did not reduce cellular respiration (Fig. 4A) or commit cells to undergo apoptosis (Fig. 3J). Interestingly, the $MDM2^{1-101}$-dependent decrease in cellular respiration was not prevented by co-treatment with SOD1 (a copper-zinc dependent enzyme localized to both the cytosol and mitochondrial inner-membrane space that resolves ROS by converting them to hydrogen peroxide; Che et al., 2016) or MitoQ (mitochondrially-targeted

small molecule anti-oxidant; Murphy 2016), suggesting MDM2-induced alterations in mitochondrial respiration were upstream of ROS production (Figs. 4B-C). Since the above relied upon exogenous MDM2, we next compared two human osteosarcoma cell lines with either normal (U-2 OS) or amplified (SJSA-1) MDM2 levels (Fig. S3B) for changes in mitochondrial respiration due to pharmacological regulation of MDM2. U-2 OS do not constitutively express detectible MDM2 protein, and therefore, short term (24 h) treatment with Nutlin-3A did not impact on mitochondrial respiration (Figs. 4D & 4F). In contrast, SJSA-1 constitutively express MDM2, demonstrate markedly less mitochondrial respiration compared to U-2 OS, and basal/maximal respiratory rates were further decreased by the addition of Nutlin-3A independently of apoptosis as zVAD-fmk treatment did not rescue the loss (*n.b.,* Nutlin-3A treatment did not cause detectible cell death in short term assays) (Figs. 4E-4F). We noted that a longer (48 h) Nutlin-3A treatment of U-2 OS cells resulted in detectible MDM2 protein and a reduction in basal and maximal respiration (Figs. S3C-G). These data suggest: (1) MDM2 disrupts mitochondrial respiration; and (2) Nutlin-3A could promote MDM2-dependent effects on mitochondrial respiration (Figs. 4A-F) and cell death (Fig. 1G).

Next, the literature was searched for potential insights to mechanistically unite these observations. We noted a publication that catalogued MDM2-interacting proteins, which also included a description of Nutlin-3A sensitive MDM2-interacting proteins (Nicholson et al., 2014). Specific to our study, the authors described that NDUFS1 (NADH:ubiquinone oxidoreductase 75 kDa Fe-S protein 1; Janssen et al., 2006) was a potential MDM2-interacting protein, and this interaction was potentially enhanced by Nutlin-3A. NDUFS1 contains three Fe-S clusters and participates in the entry and efficiency of electron (e^-) transfer within the NADH:dehyrogenase (N) module of Complex I (CI); and NDUFS1 also participates in supercomplex assembly with Complex III (CIII). Inspection of the NDUFS1 protein revealed an alpha helical domain with similiarities to how p53 binds MDM2. Using PyMOL, we created a hybrid NDUFS1/p53 domain in association with MDM2 to gain perspectives to the Nutlin-3A regulation (Fig. 4G), and the identification of MDM2 mutants for subsequent experiments. Previous experiments in figure 3 suggest that the MDM2 biology under investigation originates from within the cytosol, so we transfected H1299 with MDM2, isolated cytosolic fractions, and determined effects on NDUFS1. The cytosol normally has minimal NDUFS1, as once this nuclear-encoded mitochondrial protein is transcribed and translated, NDUFS1 is imported into

mitochondria. Interestingly, we noted a positive correlation between cytosolic MDM2 levels and endogenous NDUFS1 accumulation in the cytosol (Fig. 4H). Direct interactions between MDM2 and NDUFS1 were next determined using four approaches: *(i)* $MDM2^{WT}$ was transfected into H1299, cytosolic and nuclear extracts were prepared, subjected to anti-MDM2 immunoprecipitation, and probed for endogenous NDUFS1; *(ii)* endogenous NDUFS1 was immunopurified from H1299, GST-$MDM2^{WT}$ or GST-$MDM2^{1-101}$ was added, washed, and probed for NDUFS1-associated MDM2; *(iii)* endogenous cytosolic NDUFS1 was immunopurified from SJSA-1 cells, and probed for endogenous MDM2; and *(iv)* recombinant MDM2 binding to recombinant NDUFS1 was determined by microscale thermophoresis. Together, the results from these experiments demonstrated that MDM2 directly binds to NDUFS1 with an apparent affinity of $K_D = 1.1 \pm 0.6$ μM (Figs. 4I-L), which promotes NDUFS1 accumulation in the cytosol; and Nutlin-3A could enforce the interaction between MDM2 and NDUFS1. As the MDM2 interface with NDUFS1 was predicted on p53 binding, we also tested if p53 could displace NDUFS1 from MDM2, and observed dose-dependent release of NDUFS1 from MDM2 (Figs. S4A-D).

A mechanistic link between NDUFS1 and cellular stress leading to MDM2-dependent apoptosis is not described. Here, we hypothesized that MDM2-bound NDUFS1 provokes CI dysfunction leading to apoptosis. To test this hypothesis, we first examined the cellular consequences of NDUFS1 loss-of-function by reducing its expression by shRNA (Fig. 4M; two shRNAs were analzyed and combined); and indeed, this lead to marked decreases in mitochondrial OCR (Fig. 4N), increased mtROS production (Fig. 4O, *top panel*), and the induction of apoptosis (Fig. 4O, *bottom panel*). Based on the PyMOL structure in figure 4G, we generated a series of MDM2 mutants predicted to bind NDUFS1 with decreased affinity: MDM2 G58V, G58L, G58I, and G58F. Transient expression of the $MDM2^{G58}$ mutants revealed that $MDM2^{G58I}$ was less efficient at binding to NDUFS1 and promoting apoptosis, despite similar expression and cellular localization compared to $MDM2^{WT}$ and other $MDM2^{G58}$ mutants (Figs. 4P-Q, S4D-F). $MDM2^{G58I}$ failed to promote NDUFS1 accumulation in the cytosol (Fig. S4G) and mtROS compared to $MDM2^{WT}$, $MDM2^{1-101}$, and *NDUFS1* RNAi (Fig. 4R); and $MDM2^{G58I}$ also demonstrated reduced binding to NDUFS1 (Figs. 4S, S4E). To broaden the context of the MDM2 and NDUFS1 phenotypes, we compared *Drosophila* expressing *MDM2* or *ND-75* RNAi (equivalent to NDUFS1) under control of a wing-specific promoter (*c765gal4*). Similar to the

eye and wing data presented in figures 2M and S2H-J, MDM2 expression caused marked developmental abnormalities in the wing, all of which were phenocopied by *ND-75* RNAi (Fig. 4T). Next, we examined the relationship between mtROS production, CI dysfunction, and γH2AX staining in livers obtained from transgenic *Mdm2* mice (Jones et al., 1998). Transgenic *Mdm2* alleles promoted a gene-dosage dependent increase in mtROS and γH2AX positivity, along with a decrease in CI activity (Fig. 4U); and similar to our cell culture experiment, transgenic *Mdm2* expression lead to the cytosolic accumulation of NDUFS1 (Fig. 4V). Together, these data suggest that MDM2 regulates mtROS production by interacting with NDUFS1.

MDM2 integrates mitochondrial ROS production, genomic stress, and apoptosis through disruption of mitochondrial ETC efficiency. Next, we next investigated if MDM2 had direct effects on CI and mitochondrial respiration using two approaches: *(i)* GST-MDM2^{WT} and GST-MDM2$^{1-101}$ were directly added to permeabilized H1299, and standard Seahorse-based MitoStress and State 3 mitochondrial respiration (ADP/Malate/Pyruvate-stimulated) were analyzed (Fig. 5A); and *(ii)* GST-MDM2^{WT} and GST-MDM2$^{1-101}$ were directly added to digitonin-solubilized mitochondria, and CI assembly and association with CIII into supercomplexes (*e.g.,* CI_1+$CIII_2$, CI_2+$CIII_2$) was analyzed (Fig. 5B). Both investigations suggested that MDM2 had no direct or immediate consequences on assembled CI or supercomplexes. Using the DOX-inducible MDM2 cellular system defined in figure 1, we purified and digitonin-extracted mitochondria, and analyzed supercomplex assembly and activity. As shown in figure 5C, the induction of MDM2 caused an appreciable decrease in both CI activity, and $CI_{1/2}III_2$ supercomplex to CI_1 ratio, while non-incorporated CI and CII activities (for comparison) remained unaffected. Futhermore, we observed that MDM2 induction resulted in decreased incorporation of NDUFS1 into supercomplexes, as indicated by co-examination of ND1 (a mitochondrial-encoded essential CI protein); and for comparison, *NDUFS1* RNAi produced similar observations (Fig. 5D).

As the loss in supercomplex-mediated CI activity could be the mechanism for MDM2-induced apoptosis, we sought to circumvent this phenotype by sustaining high levels of overall CI activity with NDI1 (NADH-ubiquinone reductase H^+-translocating), the single polypeptide yeast homolog of mammalian CI (Marres et al., 1991). First, we tested if MDM2 had general consequences on mitochondrial respiration in yeast. MDM2^{WT} was stably expressed in yeast, and

the transformants were analyzed for growth in conditions requiring minimal (YPD) or maximal (YPEG) mitochondrial bioenergetics for survival (Figs. 5E-F). In all experiments, MDM2 had no general effect on mitochondrial respiration in yeast suggesting that additional factors (*i.e.,* NDUFS1) are necessary to link MDM2 and bioenergetic consequences. Using H1299 with stable-expression of NDI1, as measured by increased NADH dehydrogenase activity and resistance to rotenone (a CI toxin; Fig. 5G), we next examined if NDI1-sustained NADH dehydrogenase activity was sufficient to prevent MDM2-induced apoptosis. $H1299^{Control}$ and $H1299^{NDI1}$ cells were transiently transfected with increased amounts of $MDM2^{WT}$, and this produced similar levels of MDM2 protein and apoptosis (Fig. 5H), suggesting that the overall decrease in CI activity caused by MDM2 was unlikely to be the direct source of cellular stress.

A consequence of acute $CI_{1/2}III_2$ supercomplex disassembly is inefficient electron transport and increased ROS generation (Lopez-Fabuel et al., 2016). As this could be the upstream signal leading to MDM2-induced apoptosis, we examined CI dysfunction and ROS generation initiated by MDM2 and how the NDUFS1 binding mutant of MDM2 impacted on these phenotypes. Basal and State 3 OCR were compromised in the presence of $MDM2^{WT}$ (Figs. 5I-J), which was associated with decreased $CI_{1/2}III_2$ supercomplex activity (Fig. 5K). NADH-stimulated ROS production was highest in digitonin-extracted mitochondria and native gel-purified CI from $MDM2^{WT}$-expressing cells (Fig. 5L). In contrast, $MDM2^{G58I}$ failed to signficantly influence basal OCR, State 3 OCR, $CI_{1/2}III_2$ supercomplex activity, or NADH-stimulated ROS; and for comparison, *NDUFS1* RNAi produced similar observations to $MDM2^{WT}$ in these assays (Figs. 5I-L). Finally, we examined how mitigation of MDM2-induced mitochondrial ROS production impacted on DNA damage and apoptosis. Therefore, we examined the impact of SOD1 co-expression on $MDM2^{WT}$- and $MDM2^{1-101}$-induced mitochondrial ROS production, DNA damage, and subsequent apoptosis in H1299. As demonstrated before, $MDM2^{WT}$ or $MDM2^{1-101}$ lead to increased mitochondrial ROS, γH2AX accumulation, and apoptosis; and co-expression of SOD1 was effective in preventing the majority of these stress phenotypes (Figs. 5M-O). In parallel, we examined if treatment with MitoQ acted similar to SOD1, and the results were comparable (Figs. 5Q-S) suggesting that the mitigation of MDM2-induced mitochondrial ROS prevents MDM2-induced DNA damage and apoptosis. To evaluate specificity for MDM2-induced apoptosis, we evaluated how SOD1 and

MitoQ impacted on general commitment to apoptosis (*e.g.,* induced by staurosporine, STS), and no changes were observed (Figs. 5P, 5T).

DISCUSSION

An abundance of MDM2 binding proteins, substrates for degradation, and small molecules targeting its function highlight the impact of MDM2 in cell biology and disease. Here, we describe a novel signaling network and subsequent cellular phenotypes that result from chronic MDM2 expression. We posit that MDM2 stabilization can lead to the cytosolic accumulation of NDUFS1, which destabilizes supercomplex (*e.g.,* $CI_{1/2}$+$CIII_2$) assembly leading to marked mitochondrial ROS generation and decreased respiration (Figs. 4 & 5). If left unresolved, mitochondrial ROS can promote DNA damage eventually leading to BIM-mediated BAK/BAX-dependent activation of the mitochondrial pathway of apoptosis (Figs. 2 & 3). Cellular responses to MDM2-induced stress appear conserved across species, as developing *Drosophila* tissues, murine organs, transformed murine cell lines, and human cancer cell lines share similar phenotypes; and yet varied, as *Drosophila* tissues activate the mitochondrial pathway of apoptosis, similar to cultured cell lines, but murine liver appears to persist with minimal apoptotic responses despite increased ROS and detectable DNA damage (Figs. 2, 4, S1, S2).

Several studies have highlighted the importance of gaining a broader perspective of the MDM2 interactome, and its regulation by small molecules like Nutlin-3A (Janssen et al., 2006; Way et al., 2016). MDM2 is described to bind to over 100 proteins, yet little is known about how all these interactions relate to the cell biology of MDM2. Small molecules targeting MDM2 alter the binding of its associated proteins by either directly disrupting the MDM2 interface required for association --- and/or --- promote numerous allosteric changes in multiple MDM2 domains directly, thus altering motifs to that either gain or lose capacity to interact with proteins (Janssen et al., 2006; Way et al., 2016). Here, we noted that Nutlin-3A could enhance the interaction between MDM2 and NDUFS1 (Fig. 4J), and this promoted decreased mitochondrial respiration in cancer cells harboring amplified *MDM2* (Figs. 4D-F), and apoptosis in cells where MDM2 was introduced transiently (Fig. 1G). Numerous mitochondrial proteins (*e.g.,* mitochondrial pyruvate dehydrogenase complex) and functions (*e.g.,* nucleotide exchange and electron transport) are regulated in a Nutlin-3A-dependent manner with little mechanistic or biological insights (Janssen et al., 2006; Way et al., 2016; Schneider et al., 2016), and there are notions in the literature that Nutlin-3A can regulate both cellular metabolism and signaling independent of

the p53 pathway (Ye et al., 2017; Fåhraeus et al., 2014). A key area of future investigation is to determine under which circumstances cells promote the MDM2·NDUFS1 interaction to regulate mitochondrial respiration, and what are the upstream signals that promote MDM2 stabilization and function in these settings. Moreover, a burgeoning literature shows that MDM2 can also bind DNA, both nuclear and mitochondrial, to control cellular metabolism and disease phenotypes, such as cancer metastasis (Riscal et al., 2016; Arena et al., 2018). Within figure S1E, we noted that *MDMX* expression also has a pro-apoptotic effect, while we did not investigate the causes and consequences of this phenotype, it is curious to note that MDM2 and MDMX share marked similarities at the amino terminus that may potentially suggest shared mechanisms (Karni-Schmidt et al., 2016).

Together, our data along with the literature reveal that a deeper mechanistic interrogation of MDM2 biology and its pharmacological regulation are necessary to fully appreciate the biological and clinical applications of this important protein and pathway. Moreover, recent literature reveals that MDM2-mediated signaling captures a broad spectrum of survival and stress pathways that likely influence its contrasting oncogenic and tumor suppressor functions. While the mechanisms described by us and Arena and colleagues are distinct, yet complementary, and p53-independent, it is becoming increasingly apparent that the p53/MDM2 pathway has multiple intersections with numerous mitochondrial components --- adding further complexity, interest, and broader therapeutic potential to the oncogenic and tumor suppressor roles of p53 and MDM2 in health and disease.

ACKNOWLEDGEMENTS

We thank everyone in the Chipuk Laboratory and the Department of Oncological Sciences (especially Drs. Stuart A. Aaronson, Satish Mungamuri, Matthew O'Connell, James J. Manfredi, and Lois Resnick-Silverman). Dr. Jean-Ehrland Ricci (University of Nice Sophia Antipolis) for the pLXIN-NDUFS1 construct; Dr. Amaia Lujambio (Icahn School of Medicine at Mount Sinai) for the floxed *Trp53* MEFs*;* Dr. Stephen N. Jones (Frederick National Laboratory for Cancer Research) for access to the transgenic *Mdm2* mice; Dr. Christine Eischen (Thomas Jefferson University) for several MDM2 plasmids. The MDM2 fly strain was generously provided by Dr. Joel Silber; and many other *Drosophila* reagents were provided by the Bloomington stock center. This work was supported by: NIH grants R01 CA157740 (J.E.C.), R01 CA206005 (J.E.C.), and R01 GM12995 (C.M.P.); the JJR Foundation, the William A. Spivak Fund, the Fridolin Charitable Trust, an American Cancer Society Research Scholar Award, a Leukemia & Lymphoma Society Career Development Award, and an Irma T. Hirschl / Monique Weill Caulier Trust Research Award. This work was also supported in part by two research grants (5FY1174 and 1FY13416) from the March of Dimes Foundation, the Developmental Research Pilot Project Program within the Department of Oncological Sciences at the Icahn School of Medicine at Mount Sinai, and the Tisch Cancer Institute Cancer Center Support Grant (P30 CA196521).

AUTHOR CONTRIBUTIONS

R.E., and J.E.C. conceived the project. R.E., I.A.-E., A.P.T., C.R.P., J.N.M., M.N.S., M.P.L.-V., J.R.K., G.P.M., C.Z., S.A., C.M.P., and J.E.C. performed the experiments. J.E.C., G.P.M., and C.M.P. wrote the paper.

DECLARATION OF INTERESTS

The authors declare no competing financial interests.

REFERENCES

Arena G., Cissé M.Y., Pyrdziak S., Chatre L., Riscal R., Fuentes M., Arnold J.J., Kastner M., Gayte L., Bertrand-Gaday C., Nay K., Angebault-Prouteau C., Murray K., Chabi B., Koechlin-Ramonatxo C., Orsetti B., Vincent C., Casas F., Marine J.C., Etienne-Manneville S., Bernex F., Lombès A., Cameron C.E., Dubouchaud H., Ricchetti M., Linares L.K., and Le Cam L. (2018). Mitochondrial MDM2 Regulates Respiratory Complex I Activity Independently of p53. Mol Cell. *69*, 594-609.

Bueso-Ramos, C.E., Yang, Y., deLeon, E., McCown, P., Stass, S.A., and Albitar, M. (1993). The human MDM-2 oncogene is overexpressed in leukemias. Blood *82*, 2617-2623.

Bueso-Ramos, C.E., Manshouri, T., Haidar, M.A., Huh, Y.O., Keating, M.J., and Albitar, M. Multiple patterns of MDM-2 deregulation in human leukemias: implications in leukemogenesis and prognosis. (1995). Leuk Lymphoma *17*, 13-18.

Bueso-Ramos, C.E., Manshouri, T., Haidar, M.A., Yang, Y., McCown, P., Ordonez, N., Glassman, A., Sneige, N., and Albitar, M. (1996). Abnormal expression of MDM-2 in breast carcinomas. Breast Cancer Res Treat *37*, 179-188.

Che M., Wang R., Li X., Wang H.Y., and Zheng X.F.S. (2016). Expanding roles of superoxide dismutases in cell regulation and cancer. Drug Discov Today *1*, 143-149.

Chipuk J.E., Moldoveanu T., Llambi F., Parsons M.J., and Green D.R. (2010). The BCL-2 family reunion. Mol Cell. *37*, 299-310.

Davidson F.F., and Steller H. (1998). Blocking apoptosis prevents blindness in Drosophila retinal degeneration mutants. Nature *391*, 587-591.

Fåhraeus R., and Olivares-Illana V. (2014). MDM2's social network. Oncogene *33*, 4365-4376.

Fakharzadeh, S.S., Trusko, S.P., and George, D.L. (1991). Tumorigenic potential associated with enhanced expression of a gene that is amplified in a mouse tumor cell line. EMBO J *10*, 1565-1569.

Folberg-Blum, A., Sapir, A., Shilo, B.Z., and Oren, M. (2002). Overexpression of mouse Mdm2 induces developmental phenotypes in Drosophila. Oncogene *21*, 2413-2417.

Freedman D.A., Epstein C.B., Roth J.C., and Levine A.J. (1997). A genetic approach to mapping the p53 binding site in the MDM2 protein. Mol Med. *3*, 248-259.

Gelles J.D., and Chipuk J.E. (2016). Robust high-throughput kinetic analysis of apoptosis with real-time high-content live-cell imaging. Cell Death Dis. *7*, e2493.

Iwakuma, T. and Lozano, G. MDM2, an introduction. (2003). Mol Cancer Res *1*, 993-1000.

Janssen R.J., Nijtmans L.G., van den Heuvel L.P., and Smeitink J.A. (2006). Mitochondrial complex I: structure, function and pathology. J Inherit Metab Dis *29*, 499-515.

Jeyaraj, S., O'Brien, D.M., and Chandler, D.S. (2009). MDM2 and MDM4 splicing: an integral part of the cancer spliceome. Front Biosci *14*, 2647-2656.

Jones, S.N., Hancock, A.R., Vogel, H., Donehower, L.A., and Bradley, A. (1998). Overexpression of Mdm2 in mice reveals a p53-independent role for Mdm2 in tumorigenesis. Proc Natl Acad Sci U S A *95*, 15608-15612.

Karni-Schmidt O, Lokshin M, Prives C. The Roles of MDM2 and MDMX in Cancer. Annu Rev Pathol. 2016 May 23;11:617-44.

Kubbutat M.H., Ludwig R.L., Levine A.J., and Vousden K.H. (1999). Analysis of the degradation function of Mdm2. Cell Growth Differ. *10*, 87-92.

Lopez-Fabuel I., Le Douce J., Logan A., James A.M., Bonvento G., Murphy M.P., Almeida A., and Bolaños J.P. (2016). Complex I assembly into supercomplexes determines differential mitochondrial ROS production in neurons and astrocytes. Proc Natl Acad Sci U S A. *113*, 13063-13068.

Manfredi J.J. (2010). The Mdm2-p53 relationship evolves: Mdm2 swings both ways as an oncogene and a tumor suppressor. Genes Dev. *24*, 1580-1589.

Marres C.A., de Vries S., and Grivell L.A. (1991). Isolation and inactivation of the nuclear gene encoding the rotenone-insensitive internal NADH: ubiquinone oxidoreductase of mitochondria from Saccharomyces cerevisiae. Eur J Biochem. *195*, 857-862.

Matsumura, T., Yoshihama, Y., Kimura, T., Shintani, S., and Alcalde, R.E. (1996). P53 and MDM2 expression in oral squamous cell carcinoma. Oncology *53*, 308-312.

Momand, J., Zambetti, G.P., Olson, D.C., George, D., and Levine, A.J. (1992). The mdm-2 oncogene product forms a complex with the p53 protein and inhibits p53-mediated transactivation. Cell *69*, 1237-1245.

Murphy M.P. (2016). Understanding and preventing mitochondrial oxidative damage. Biochem Soc Trans. *44*, 1219-1226.

Nicholson J., Scherl A., Way L., Blackburn E.A., Walkinshaw M.D., Ball K.L., and Hupp T.R. (2014). A systems wide mass spectrometric based linear motif screen to identify dominant in-vivo interacting proteins for the ubiquitin ligase MDM2. Cell Signal. *26*, 1243-1257.

Oliner, J.D., Kinzler, K.W., Meltzer, P.S., George, D.L. and Vogelstein, B. (1992). Amplification of a gene encoding a p53-associated protein in human sarcomas. Nature *358*, 80-83.

Oltersdorf T., Elmore S.W., Shoemaker A.R., Armstrong R.C., Augeri D.J., Belli B.A., Bruncko M., Deckwerth T.L., Dinges J., Hajduk P.J., Joseph M.K., Kitada S., Korsmeyer S.J., Kunzer A.R., Letai A., Li C., Mitten M.J., Nettesheim D.G., Ng S., Nimmer P.M., O'Connor J.M., Oleksijew A., Petros A.M., Reed J.C., Shen W., Tahir S.K., Thompson C.B., Tomaselli K.J., Wang B., Wendt M.D., Zhang H., Fesik S.W., and Rosenberg S.H. (2005). An inhibitor of Bcl-2 family proteins induces regression of solid tumours. Nature *435*, 677-681.

Reifenberger, G., Liu, L., Ichimura, K., Schmidt, E.E., and Collins, V.P. (1993). Amplification and overexpression of the MDM2 gene in a subset of human malignant gliomas without p53 mutations. Cancer Res *53*, 2736-2739.

Renault T.T., Luna-Vargas M.P., and Chipuk J.E. (2016). Mouse Liver Mitochondria Isolation, Size Fractionation, and Real-time MOMP Measurement. Bio Protoc. *6*, pii: e1892.

Riscal R., Schrepfer E., Arena G., Cissé M.Y., Bellvert F., Heuillet M., Rambow F., Bonneil E., Sabourdy F., Vincent C., Ait-Arsa I., Levade T., Thibaut P., Marine J.C., Portais J.C., Sarry J.E., Le Cam L., and Linares L.K. (2016). Chromatin-Bound MDM2 Regulates Serine Metabolism and Redox Homeostasis Independently of p53. Mol Cell. *62*, 890-902.

Saadatzadeh M.R., Elmi A.N., Pandya P.H., Bijangi-Vishehsaraei K., Ding J., Stamatkin C.W., Cohen-Gadol A.A., and Pollok K.E. (2017). The Role of MDM2 in Promoting Genome Stability versus Instability. Int J Mol Sci. *18*, ppi2216.

Schneider L.S., Ulrich M., Lehr T., Menche D., Müller R., and von Schwarzenberg K. (2016). MDM2 antagonist nutlin-3a sensitizes tumors to V-ATPase inhibition. Mol Oncol. *7*, 1054-1062.

Singh, R.K., Tapia-Santos, A., Bebee, T.W., and Chandler, D.S. (2009). Conserved sequences in the final intron of MDM2 are essential for the regulation of alternative splicing of MDM2 in response to stress. Exp Cell Res *315*, 3419-3432.

Tan B.X., Liew H.P., Chua J.S., Ghadessy F.J., Tan Y.S., Lane D.P., and Coffill C.R. (2017). Anatomy of Mdm2 and Mdm4 in evolution. J Mol Cell Biol. *9*, 3-15.

Way L., Faktor J., Dvorakova P., Nicholson J., Vojtesek B., Graham D., Ball K.L., and Hupp T. (2016). Rearrangement of mitochondrial pyruvate dehydrogenase subunit dihydrolipoamide dehydrogenase protein-protein interactions by the MDM2 ligand nutlin-3. Proteomics. *17*, 2327-2344.

White K., Grether M.E., Abrams J.M., Young L., Farrell K., and Steller H. (1994). Genetic control of programmed cell death in Drosophila. Science *264*, 677-683.

Wittig I., Karas M., and Schägger H. (2007). High resolution clear native electrophoresis for in-gel functional assays and fluorescence studies of membrane protein complexes. Mol Cell Proteomics. *6*, 215-225.

Vassilev L.T., Vu B.T., Graves B., Carvajal D., Podlaski F., Filipovic Z., Kong N., Kammlott U., Lukacs C., Klein C., Fotouhi N., and Liu E.A. (2004). In vivo activation of the p53 pathway by small-molecule antagonists of MDM2. Science *303*, 844-848.

Vousden, K.H., and Prives, C. (2005). P53 and prognosis: new insights and further complexity. Cell *120*, 7-10.

Ye C., Tang H., Zhao Z., Lei C.T., You C.Q., Zhang J., Gao P., He F.F., Chen S., Wang Y.M., Zhang C., and Su H. (2017). MDM2 mediates fibroblast activation and renal tubulointerstitial fibrosis via a p53-independent pathway. Am J Physiol Renal Physiol. *312*, F760-F768.

FIGURE TITLES AND LEGENDS

Figure 1. MDM2 regulates cellular survival independent of its canonical functions.

(A) H1299 were transfected with pCMV-MDM2^{WT} (0.1, 0.25, 0.5 μg), cultured for 48 hours, and dead cells were quantified by AnnexinV staining and flow cytometry. Whole cell lysates were analyzed by SDS-PAGE and western blot for indicated proteins. β-Actin is the loading control.

(B) H1299 were infected with retroviral shRNA constructs to silence *MDMX*, and then transfected with pCMV-MDM2 (0.25 μg). Cell death and *MDMX* expression were quantified by flow cytometry and qPCR, respectively.

(C) H1299 were transfected with pCMV-MDM2^{WT} (0.1, 0.2, 0.3, 0.4, 0.5 μg) or pCMV-MDM2^{C464A} (0.01, 0.02, 0.03, 0.04, 0.05 μg), cultured for 48 hours, and evaluated as in *A*. *N.B.,* MDM2^{C464A} does not self-ubiquitinylate leading to constitutive degradation; therefore, ~10× less cDNA produces similar protein levels compared to MDM2^{WT}.

(D) H1299 were transfected with pcDNA3.1-p53^{WT} and/or pCMV-MDM2^{WT} (0.25 μg each), cultured for 48 hours, and evaluated as in *A*.

(E) Indicated cells were transfected with pCMV-MDM2^{WT} (0.1, 0.25, 0.5 μg), and evaluated as in *A*.

(F) H1299 were transfected with pCMV-MDM2^{WT} or pCMV-MDM2^{G58A} (0.25 μg each), cultured for 48 hours, and evaluated as in *A*.

(G) H460 and H23 were transiently transfected with pCMV-MDM2^{WT} (0.5 μg), cultured for 24 hours, treated with Nutlin-3A (1 μM) for 48 hours, and dead cells were quantified by AnnexinV staining and flow cytometry.

(H - I) H1299 stably expressing pTRE2-MDM2^{TetOn} were treated with doxycycline (1 μg/ml) for indicated times. Cell death and MDM2 expression were determined by flow cytometry (*H*) and western blot (*I*), respectively. CD95/FAS ligation with the antibody CH11 is a positive control for cell death.

All data are representative of at least three independent experiments, and reported as ± S.D., as required.

Figure 2. MDM2-induced cell death is engaged by the mitochondrial pathway of apoptosis.

(A) H1299 were transfected with pCMV-MDM2^{WT} or pCMV-HDM2^{WT} (0.25 μg each), cultured for 48 hours, and dead cells were quantified by AnnexinV staining and flow cytometry. Whole cell lysates were analyzed by SDS-PAGE and western blot for indicated proteins. β-Actin is the loading control.

(B) H1299 were transfected with pCMV-MDM2^{WT} (0.25 μg), cultured for 48 hours, and nuclei were labeled with DAPI before live-cell fluorescent microscopy. Scale bar = 10 μm.

(C) H1299 were transfected with pCMV-MDM2^{WT} (0.25 μg) ± zVAD-fmk (100 μM), and the kinetics of cell death were detected using an IncuCyte Zoom.

(D) Same as *C*, but cells were transfected with pCMV-MDM2^{WT} (0.1, 0.25, 0.5 μg), ± zVAD-fmk (100 μM), and the kinetics of cell death were detected using an IncuCyte Zoom. Endpoint data for 48 hours are shown.

(E) H1299 were transfected with pCMV-MDM2^{WT} (0.1, 0.25, 0.5 μg), and colony formation was quantified 7 days later.

(F) H1299 were transfected with pCMV-FADD-DN (0.5 μg) and/or pCMV-MDM2^{WT} (0.25 μg), cultured for 48 hours, and apoptotic cells were quantified. CH11 (1 μg/ml; 24 hours) was used as a positive control for apoptosis.

(G) H1299 were transfected with pCMV-MDM2^{WT} (0.1, 0.25, 0.5 μg), and whole cell lysates were analyzed by western blot for indicated proteins.

(H) H1299 were transfected with pCMV-MDM2^{WT} (0.5 μg), whole cell and mitochondrial extracts isolated, and analyzed for indicated proteins. VDAC and β-Actin are the loading controls.

(I - J) H1299 stably expressing *BIM* RNAi (*I*) or *BAX* RNAi (*J*) were transfected with pCMV-MDM2^{WT} (0.1, 0.25, 0.5 μg), cultured for 48 hours, and apoptotic cells were quantified.

(K) H1299 were transfected with pCMV-MDM2^{WT} (0.1, 0.25, 0.5 μg) ± pcDNA3-hBCL-xL (1μg) or pcDNA3.1-hMCL-1 (1 μg), cultured for 48 hours, and dead cells were quantified.

(L) H1299 were transfected with pCMV-MDM2^{WT} (0.1, 0.25, 0.5 μg) ± ABT-737 (1 μM), cultured for 48 hours, and apoptotic cells were quantified.

(M) Representative images of *Drosophila* expressing transgenic *MDM2* using the eye-specific *GMRgal4*. "MDM2" = 1 copy of *GMR>MDM2*; "MDM2 × 2" = 2 copies of *GMR>MDM2*; "Control" is *GMRgal4/+*. Studies were performed at 21°C; female eyes are shown.

(N) Representative images of transgenic *GMR>MDM2* flies with *H99* deletion, or co-expressing *DIAP1* or *p35*. Studies were performed at 25°C; female eyes are shown.

(O) Quantification of eclosed progeny from parallel crosses from *M* and *N* performed at 30°C compared to the percent of each genotype expected for Mendelian inheritance.

All data are representative of at least three independent experiments, and reported as ± S.D., as required.

Figure 3. The MDM2 amino terminal domain (amino acids 1-101) is sufficient to promote the mitochondrial pathway of apoptosis and causes genomic and oxidative stress.

(A) Schematic of MDM2 variants used in this study.

(B - C) H1299 were transfected with indicated MDM2 variants (0.25 μg each), cultured for 48 hours, and apoptotic cells were quantified by AnnexinV staining and flow cytometry (*B*). Whole cell lysates were analyzed by SDS-PAGE and western blot for indicated proteins. β-Actin is the loading control (*C*).

(D) H1299 were transfected with pCMV-MDM2$^{1-227}$ (0.5 μg) ± ABT-737 (1 μM) or ± zVAD-fmk (100 μM), cultured for 48 hours, and apoptotic cells were quantified.

(E) H1299 were transfected with pCMV-MDM2$^{1-227}$ (0.5 μg) ± pcDNA3-hBCL-xL (1 μg), cultured for 48 hours, and apoptotic cells were quantified.

(F) H1299 were transfected with pCMV-MDM2$^{1-101}$ (0.1, 0.25, 0.5 μg), ± zVAD-fmk (100 μM), cultured for 48 hours, and apoptotic cells were quantified. Whole cell lysates were analyzed by SDS-PAGE and western blot for indicated proteins.

(G) H1299 were transfected with pCMV-MDM2^{WT} or pCMV-MDM2$^{1-101}$ (0.25 μg) in the presence of zVAD-fmk (100 μM), cultured for 24 hours, fixed, and stained for MDM2 localization. Scale bar = 20 μm. > 200 cells were analyzed for each condition, and the % indicated.

(H) Same as *G*, but comparing pCMV-MDM2^{WT}, pCMV-MDM2^{NES-}, or pCMV-MDM2^{NLS-}. Scale bar = 10 μm. > 200 cells were analyzed for each condition, and the % indicated.

(I) Same as *G-H*, but whole cell lysates were analyzed by western blot for indicated proteins.

(J) H1299 were transfected with pCMV-MDM2^{WT}, pCMV-MDM2^{NES-}, or pCMV-MDM2^{NLS-} (0.25 or 0.5 μg each), cultured for 48 hours, and apoptotic cells were quantified.

(K) H1299 transfected with pCMV-MDM2^{WT}, pCMV-MDM2^{NES-}, or pCMV-MDM2$^{1-101}$ (0.25 μg), fixed, and labeled with an γH2AX antibody and DAPI. Scale bar = 10 μm. > 200 cells were analyzed for each condition, and the % indicated.

(L) H1299 were treated with VP16 (25 μM) or transfected with pCMV-MDM2$^{1-101}$ (0.25 μg), cultured for 24 hours, and harvested for western blot analysis.

(M) H1299 were transfected with pCMV-MDM2^{WT} or pCMV-MDM2$^{1-101}$ (0.25 μg), and analyzed for metaphase spreads. Arrows indicate chromosomal aberrations.

(N - O) H1299 were transfected with indicated MDM2 variants (0.25 μg), cultured for 24 hours, loaded with either CellROS (1 μM) or MitoSOX (5 μM), analyzed by flow cytometry, and reported as relative fluorescent units (RFU).

All data are representative of at least three independent experiments, and reported as ± S.D., as required.

Figure 4. MDM2 binds NDUFS1 to destabilize supercomplex-assembled Complex I and promote ROS.

(A) H1299 were transfected with pCMV-MDM2^{WT}, pCMV-MDM2^{NES-}, pCMV-MDM2^{NLS-}, or pCMV-MDM2$^{1-101}$ (0.25 μg), cultured for 24 hours, and subjected to Seahorse XF Cell Mito Stress analysis.

(B) H1299 were transfected with pCMV-MDM2$^{1-101}$ (0.25 μg) in the presence of SOD1-GFP (0.25 μg) or MitoQ (5 μM), cultured for 24 hours, and subjected to Seahorse XF Cell Mito Stress analysis.

(C) Relative basal and maximal oxygen consumption rates from *B* are presented.

(D - E) U-2 OS *(D)* and SJSA-1 *(E)* cells were treated with zVAD-fmk (100 μM) ± Nutlin-3A (1 μM) for 24 hours, and subjected to Seahorse XF Cell Mito Stress analysis.

(F) Relative basal and maximal oxygen consumption rates from *D & E* are presented.

(G) A p53 peptide (PDB: 4hfz, residues 17-27, dark blue) was integrated within an NDUFS1 α-helix (PDB: 5gup, residues 617-632, magenta), and complexed with MDM2 (PDB: 4hfz, residues 26-108, grey) using PyMOL. The NDUFS1 residues W620, K621, and I623 are highlighted in stick representation and form the consensus sequence for MDM2 binding.

(H) H1299 were transfected with pCMV-MDM2^{WT} (0.1, 0.25, 0.5, 1 μg) for 24 hours in the presence of zVAD-fmk (100 μM), and cytosolic extracts were analyzed by SDS-PAGE and western blot.

(I) H1299 were transfected with pCMV-MDM2^{WT} (1 μg) for 24 hours in the presence of zVAD-fmk (100 μM), nuclear and cytosolic extracts were subjected to anti-MDM2 immunoprecipitation, and complexes were analyzed by western blot for indicated proteins.

(J) Endogenous NDUFS1 was immuno-purified from H1299, GST-MDM2^{WT} or GST-MDM2$^{1-101}$ was added (0.1 μg) ± Nutlin-3A (1 μM), incubated, washed, and the complexes were analyzed by western blot for indicated proteins.

(K) Cytosolic lysates from SJSA-1 were subjected to anti-NDUFS1 immunoprecipitation, and complexes were analyzed by western blot for indicated proteins.

(L) GST, GST-MDM2^{WT}, and GST-MDM2$^{1-101}$ were analyzed by microscale thermophoresis for binding to human NDUFS1. K_d values are listed. The human p53 peptide a.a. 17 - 26 is a positive control for MDM2 binding.

(M) H1299 were infected with shRNA against *NDUFS1* (or control) for 96 hours. Total RNA and protein were analyzed by qPCR and western blot for *NDUFS1* knock-down efficiency, respectively.

(N) Cells in *M* were analyzed by Seahorse for MitoStress.

(O) H1299 were infected with shRNA against *NDUFS1* (or control) for 96 hours; and mitochondrial ROS production was measured with MitoSOX *(top panel)* or apoptotic cells were quantified 48 hours later *(bottom panel)*. FCCP (1 μM) is a positive control for both assays.

(P - Q) H1299 were transfected with indicated MDM2 mutants (1 μg each), cultured for 48 hours, and apoptotic cells were quantified by AnnexinV staining and flow cytometry (*P*). Whole cell lysates were analyzed by SDS-PAGE and western blot for indicated proteins. β-Actin is the loading control.

(R) H1299 were infected with shRNA against *NDUFS1* (or control) for 96 hours; or transfected with pCMV-MDM2^{WT} or pCMV-MDM2$^{1-101}$ (1 μg) for 48 hours in the presence of zVAD-fmk (100 μM), mitochondrial ROS production was measured with MitoSOX and reported as relative fluorescent units (RFU).

(S) H1299 were transfected with pCMV-MDM2^{WT} or pCMV-MDM2^{G58I} (1 μg each) for 24 hours in the presence of zVAD-fmk (100 μM), cytosolic extracts were subjected to anti-MDM2 (or anti-NDUFS1) immunoprecipitation, and complexes were analyzed by western blot for indicated proteins.

(T) Representative images of *Drosophila* expressing an inverted repeat to induce *ND75* RNAi (*c765>ND-75^{IR}*) at 18°C or transgenic *MDM2* (*c765>MDM2*) at 21°C under control of the wing-specific *c765* promoter. "*c765gal4/+*" is the control wing.

(U) Livers from wild-type (*Wt/Wt*), *MDM2^{Tg}* × 1 allele (*Wt/Tg*), and *MDM2^{Tg}* × 2 alleles (*Tg/Tg*) animals were analyzed for mtROS generation, Complex I activity, and γH2AX foci. All activities were normalized against *Wt/Wt* (set to 100), and reported as "Relative Units".

(V) Total, cytosolic, and mitochondrial fractions from fresh livers harvested from the indicated genotypes were analyzed for indicated proteins. *Wt/Tg* often displayed variable levels of MDM2 protein, and two examples are shown. "+" indicates a lane with mitochondrial lysate as a positive control.

All data are representative of at least three independent experiments, and reported as ± S.D., as required.

Figure 5. MDM2 integrates mitochondrial ROS production, genomic stress, and apoptosis through disruption of mitochondrial ETC efficiency.

(A) Pyruvate/malate/ADP-stimulated CI activity *(top panel)* and FCCP-induced maximal respiration *(bottom panel)* were determined with a Seahorse Analyzer using permeabilized H1299 cells treated with buffer, MDM2^{WT} (10 μM), or MDM2$^{1-101}$ (10 μM).

(B) H1299 mitochondrial fractions were digitonin extracted, treated with buffer, MDM2^{WT} (10 μM), or MDM2$^{1-101}$ (10 μM), and subject to blue native gel electrophoresis (BNGE) for indicated ETC assembly, in-gel Complex I (IG-CI), and in-gel Complex II (IG-CII) activities.

(C) H1299 stably expressing pTRE2-MDM2^{TetOn} were treated with doxycycline (1 μg/ml) for 48 hours in the presence of zVAD-fmk (100 μM), mitochondrial fractions were digitonin extracted, and analyzed as in *B*.

(D) Mitochondrial fractions from H1299 infected with shRNA against *NDUFS1* and H1299 stably expressing pTRE2-MDM2^{TetOn} (treated as in *C*) were digitonin-extracted, and analyzed by

native gel electrophoresis/western blot and SDS-PAGE/western blot for indicated proteins. CII and β-Actin are loading controls.

(E) Total protein extracts from the indicated yeast transformants were precipitated and analyzed by SDS-PAGE and western blot.

(F) Indicated transformants were serially diluted and plated on either YDP or YPEG, and incubated for 3 days at 30°C. W303ΔCOA2 is a strain deficient in COA2, an assembly factor for cytochrome *c* oxidase.

(G) H1299 stably expressing NDI1 was examined with a Seahorse Analyzer for increased CI function *(top panel)*, and resistance to rotenone (50 nM, or DMSO) induced loss of clonogenic survival *(bottom panel)*.

(H) Cells in *G* were transfected with pCMV-MDM2^{WT} (0.1, 0.25, 0.5 μg; or pCMV), and whole cell lysates were analyzed by western blot for indicated proteins *(top panel)*; or cells were cultured for 48 hours and apoptotic cells were quantified *(bottom panel)*.

(I) H1299 stably expressing pTRE2-^{TetOn} (Control, MDM2^{WT}, or MDM2^{G58I}) treated with doxycycline (1 μg/ml) for 48 hours in the presence of zVAD-fmk (100 μM), or H1299 infected with shRNA against *NDUFS1*, were analyzed with a Seahorse Analyzer for basal and Pyruvate/malate/ADP-stimulated (State3) respiration. A representative dataset is shown.

(J) Data in *I*, presented as relative units (RU).

(K) Digitonin-extracted mitochondria from cells described in *I* were analyzed by IG-CI and IG-CII assays.

(L) NADH-stimulated ROS production was measured in digitonin-extracted mitochondria from cells described in *I (top panel)*, and following BNGE and elution of CI *(bottom panel)*.

(M) H1299 were transfected with pCMV-MDM2^{WT} or pCMV-MDM2$^{1-101}$ (0.25 μg) ± pEGFP-SOD1 (1 μg), cultured for 24 hours, loaded MitoSOX (5 μM), and analyzed by flow cytometry.

(N) H1299 were transfected with pCMV-MDM2^{WT} or pCMV-MDM2$^{1-101}$ (0.25 μg), fixed, and labeled with an γH2AX antibody and DAPI. 100 cells per condition were quantified, in three independent.

(O) H1299 were transfected with pCMV-MDM2^{WT} or pCMV-MDM2$^{1-101}$ (0.25 μg) ± pEGFP-SOD1 (1 μg), cultured for 48 hours, and apoptotic cells were quantified.

(P) H1299 were transfected with pEGFP-SOD1 (1 μg), cultured for 48 hours, treated with staurosporine (250 nM), and apoptotic cells were quantified 20 hours later.

(Q - T) Same as *M-P*, except studies were performed in the presence of MitoQ (5 μM).

All data are representative of at least three independent experiments, and reported as ± S.D., as required.

METHODS

Reagents. All cell culture reagents were from Invitrogen; and standard laboratory reagents were from Sigma-Aldrich or Fisher Scientific. Drugs were from: ABT737 (Abbvie); Antimycin A, Etoposide, FCCP, Nutlin-3a, Staurosporine (Sigma-Aldrich); zVAD-fmk (VWR Scientific); MitoQ (MedKoo Biosciences). Antibodies (clone or source): β-Actin (C4), BCL-2 (100), CH11 (Millipore), BAK (G23), BAX (N20), BCL-xL (S18), MDM2 (SMP14), p53 (DO-1), BCL-2 (100), BIM (22-40), p21 (C19), pH2AX (JBW301), SOD1 (FL154), Cyclin D1 (Cell Signaling), Chk1 (FL476, Cell Signaling), Chk1Ser317 (Cell Signaling), Chk1Ser345 (Cell Signaling), GST (Z-5), NDI (C-18, Santa Cruz), NDUFS1 (E-8, Santa Cruz), VDAC (FL-283, Santa Cruz), Cytochrome c (7H8, Santa Cruz). CellROX® and MitoSOX^{TM} were from Thermo Fisher Scientific, and Hoechst 33342 was from Anaspec.

Cell culture, apoptosis assays, and clonogenic survival. H1299, A549, H23, H460, U-2 OS, 293T, and MEF lines were cultured in Dulbecco's modified Eagle's medium containing 10% heat inactivated fetal bovine serum, 2 mM L-glutamine, 100 U/mL penicillin and 100 μg/mL streptomycin. SJSA-1 and HCT116 cells were cultured in Roswell Park Memorial Institute Medium (RPMI) and McCoy's 5A Medium, respectively, with the same supplements. For flow cytometry-based cell death studies, cells were seeded for 24 hours, treated as described, floating and attached cells harvested, labeled with AnnexinV-FITC in binding buffer (10 mM HEPES pH 7.4, 150 mM NaCl, 5 mM KCl, 1 mM $MgCl_2$, 1.8 mM $CaCl_2$), and analyzed by flow cytometry as indicated. For most clonogenic survival studies, cells were seeded for 24 hours, treated as indicated for 24 hours before changing the media, and cultured for seven days. For comparisons between parental and NDI1 over-expressing clones, cells were treated every two days with either DMSO or rotenone until the DMSO-treated cells reached confluency. Colonies were stained with 0.1% methylene blue and imaged. Colonies were then de-stained (20% methanol in 5% acetic acid), and the supernatant was measured for absorption at 668 nm for relative quantification of colony numbers. All transfections were performed using Lipofectamine 2000 according to the instructions, and empty pcDNA3.1 or pCMV were used as control vectors in all conditions.

Plasmids. pCMV-MDM2^{WT}, pCMV-MDM2^{C464A}, and pCMV-HDM2^{WT} were generous gifts from Dr. James J. Manfredi (Icahn School of Medicine at Mount Sinai). pcDNA3.1-human p53, pcDNA3-hBCL-xL, pcDNA3.1-hMCL-1, pCMV-FADD-DN were gifts from Dr. Douglas

Green (St. Jude Children's Research Hospital). pcDNA3.1-MDM2 truncation mutants were obtained from Dr. Christine Eischen (Thomas Jefferson University). $MDM2^{G58A}$, $MDM2^{1-101}$, $MDM2^{NLS}$, and $MDM2^{NES-}$ were generated by site-directed mutagenesis of pCMV-$MDM2^{WT}$ using QuikChange II Site-Directed Mutagenesis Kit (Agilent). SOD1-GFP was a gift from Dr. Doris Germain (Icahn School of Medicine at Mount Sinai). shRNA lentiviral plasmids against *MDMX*, *Trp53*, *BAX*, and *BIM* were purchased from Sigma-Aldrich. pGEX-4T3 was used to generate pGEX-4T3-$MDM2^{WT}$ and pGEX-4T3-$MDM2^{1-101}$ for recombinant protein expression and production using standard 6X-histidine chromatography and gel filtration.

Western blot analyses. Whole cell protein lysates were made from trypsinized cells, pelleted, resuspended in RIPA buffer (50 mM Tris, pH 8.0, 150 mM NaCl, 1.0% NP-40, 0.5% sodium deoxycholate, 0.1% sodium dodecyl sulfate) supplemented with protease inhibitors (HALT, Pierce Biotechnology), incubated on ice for 10 minutes and centrifuged for 10 minutes at 21,000 × *g*. Lysates were then adjusted with RIPA buffer to equal the protein concentrations. Proteins (25 - 50 μg/lane) were subjected to SDS-PAGE before transferring to nitrocellulose by standard western conditions, blocked in 5% milk/TBST and primary antibodies (1:1000 in blocking buffer; incubated overnight at 4°C). The secondary antibody (1:5000 in blocking buffer) was incubated at 25°C for 1 hour before standard enhanced chemiluminescence detection.

Immunofluorescence. Cell were plated in Nunc™ Lab-Tek™ chamber slides and treated as indicated. Cells were washed in 1× PBS then fixed with 4% formaldehyde for 30 minutes at room temperature. Cells were washed in 1× PBS and subsequently permeabilized and blocked in 1× PBS supplemented with 5% normal goat serum and 0.3% TritonX-100 for 60 minutes at room temperature. Primary antibodies were diluted in blocking solution as follows: anti-γH2AX 1:500 (Millipore, JBW301), anti-MDM2 1:250 (SMP-14). Samples were incubated in primary antibody overnight at 4ºC. Secondary antibodies: Alexa Fluor® 488 (1:1000, Cell Signaling) and Alexa Fluor® (1:200, Cell Signaling) were diluted in blocking buffer and incubated for 90 minutes at room temperature. Samples were washed three times in 1× PBS then mounted with ProLong® Gold Antifade Reagent containing DAPI and cured overnight at room temperature. All imaging was performed at 40× magnification with a Zeiss Imager.Z1 equipped with a N-Achroplan 40×/0.75 water immersion lens and an AxioCAM MRm digital camera; images were captured using AxioVision 4.8 and Zeiss Zen software. For quantitative assays, 100 nuclei were

counted per condition and reported, in three independent experiments.

Mitochondrial ROS production and cellular ROS production analyses by flow cytometry. Cells were seeded for 24 hours, and treated as indicated. CellROX® (1 μM) or MitoSOX™ (1 μM) was added to the media, and the plates were incubated at 37ºC in the dark for 25 minutes. The cells were then trypsinized and analyzed by flow cytometry.

Microscale thermophoresis. Recombinant GST-tagged MDM2 full length and GST protein were *N*-hydroxysuccinimide (NHS) ester-modified and fluorescently labeled with Alexa Fluor 647. GST-MDM^{WT} and GST were incubated with Nutlin-3A (80 μM – 2 nM), p53 peptide (a.a. 17-26, ETFSDLWKLL, Anaspec) (125 μM – 15 nM), and NDUFS1 (63 μM – 2 nM) in MST buffer (20 mM HEPES pH 7.4, 150 mM NaCl, and 0.05% Tween-20). MicroScale Thermophoreses measurements were performed with a NanoTemper Monolith NT.115 using standard procedures.

Recombinant protein production. GST-MDM2^{WT}, GST-MDM2$^{1-101}$, and GST were expressed in *E. coli* BL21(DE3) Codon Plus (Agilent). Cells were grown in Terrific Broth media at 37ºC to an OD_{600} of ~2-3 before induction with 1 mM isopropyl-1-thio-β-D-galactopyranoside and 0.3 mM $ZnSO_4$ for 16 hours at 15ºC. All purification steps were performed at 4ºC. Cells were resuspended in lysis buffer (20 mM Tris pH 8.0, 500 mM NaCl, 5% glycerol, and 0.1 mM 4-(2-Aminoethyl)-benzenesulfonylfluoride and sonicated. Proteins were captured using a GSTrap FF column (GE HealthCare), washed in GSTrap FF lysis buffer, and eluted in lysis buffer containing 50 mM glutathione (reduced) pH 8.0. Eluted proteins were subjected to size exclusion chromatography using a Superdex S200 16/600 column in gel filtration buffer (20 mM Tris pH 8.0, 150 mM NaCl, 5% glycerol, and 1 mM TCEP). Positive peak fractions were pooled, concentrated to 5 mg/ml using Pierce Protein concentrator 10K (Thermo Scientific), aliquoted, flash frozen in liquid nitrogen, and stored at -80ºC. Human GST-NDUFS1 was purified using the same protocol.

Seahorse bioanalyzer MitoStress analysis. Cells were seeded in 200 μl DMEM complete media in XF96 plates (Agilent Technologies); plating densities: SJSA-1 4×10^3, H1299 8×10^3, MEFs 5×10^3, and treated as indicated. Oxygen consumption rates (OCR) and extracellular acidification rates (ECAR) were measured using the XF96 Extracellular Flux Analyzer and the XF Cell Mito Stress Test kit. At the end of the assay, media was removed and cells were stained with methylene blue, de-stained, and the absorbance was measured at 668 nm using a plate

reader (Synergy H1 Hybrid multi-mode micro-plate reader, BioTek). The OCR and ECAR measurements were normalized against the cell densities. Each experiment contained three independent data points. To measure FCCP-induced maximal respiration in permeabilized cells treated with recombinant MDM2, the final concentration of oligomycin was 2 μM.

Seahorse bioanalyzer complex I activity. H1299 cells were seeded in XFe96 plates (15,000 cells/well). Media was removed and cells were washed in 1× Mitochondrial Assay Buffer (MAB: 220 mM mannitol, 70 mM sucrose, 10 mM KH_2PO_4, 5 mM $MgCl_2$, 2 mM HEPES, 1 mM EGTA, 0.2% fatty acid free BSA). Cells were permeabilized in 1× MAB containing 1 nM plasma membrane permeabilizer (Agilent), and incubated at 37°C without CO_2 for 30 minutes. Baseline OCR measurements were recorded before administration of complex I metabolites and recombinant MDM2 protein. Complex I activity was measured by the administration of 10 mM pyruvate, 0.5 mM malate, 4 mM ADP ± 10 μM GST-$MDM2^{WT}$ or GST-$MDM2^{1-101}$.

Real-time live-cell analyses. H1299 were seeded at 3×10^3 cells/well in 96-well tissue culture-treated plates. Briefly, media was replaced 18 - 24 hours post plating with phenol red-free media containing the indicated treatments and fluorescently labeled recombinant Annexin V (1 μg/mL). Immediately following treatment, plates were analyzed in real time by an IncuCyte ZOOM (Essen Bioscience, Ann Arbor, MI, USA). Phase contrast and fluorescent images were captured at regular intervals using the following IncuCyte ZOOM filter cubes: Green Channel – Excitation 460 nm [440,480], Emission 524 nm [504,544]. Experiments utilized potent apoptotic inducers (250 nM staurosporine or 100 ng/ml TNFα + 25 μg/ml Cycloheximide; data not shown) as internal controls to set appropriate Y-axis values. Fluorescent events were analyzed by the IncuCyte ZOOM software as previously described (Gelles and Chipuk, 2016). A processing definition for Annexin V-FITC-labeled H1299 cells was defined as follows: Channel: Green; Top-Hat; Radius: 25 μM, Threshold: 3.0 GFU; Edge Sensitivity: -24; Pixel Adjust: 0; Area: >75 μm; Eccentricity: undefined; Mean Intensity: undefined; Integrated Intensity: undefined.

Real-time quantitative PCR. Total cellular RNA was extracted using an RNeasy kit (Qiagen) according to the manufacturer's instructions. Total RNA (1 μg) was used to synthesize first strand cDNA using the SuperScript™ III First-Strand Synthesis System for RT-PCR (Invitrogen). Gene expression was analyzed using the SYBR Green detection system (FastStart Universal SYBR Green Master, Roche) and Applied Biosciences ViiA™ 7 Real-Time PCR

system, using the comparative C_T method. The expression of relevant genes was normalized to *18S* and *gapdh*. The following primer pairs (5' - 3') were used:

RNA interference. Plasmids for shRNA were purchased from Sigma-Aldrich (Mission^R shRNA). The pLKO empty vector and scrambled shRNA constructs were kindly provided by the laboratory of Dr. E. Premkumar Reddy (Icahn School of Medicine at Mount Sinai). The 293T cell line was used to produce retroviral and lentiviral particles for the generation of stable cell lines. Virus was harvested at 24 hours and 48 hours, pooled, and 0.45 μm filtered. Stable clones were generated using puromycin (0.4 - 0.8 μg/mL).

Mitochondria isolations. As previously described, at least 2 × 15 cm dishes at 90 - 95% confluency were used per treatment (Renault et al., 2015). Cells were harvested by trypsinization, and pelleted by centrifugation at 1000 × *g* for 10 minutes. The cell pellet was washed once with mitochondrial isolation buffer (MIB: 200 mM mannitol, 68 mM sucrose, 10 mM HEPES-KOH pH 7.4, 10 mM KCl, 1 mM EDTA, 1 mM EGTA, 0.1% BSA), and resuspended in MIB supplemented with protease inhibitors (HALT, Pierce Biotechnology). The cell suspension was incubated on ice for 20 minutes, and homogenized using a 2 mL Potter-Elvehjem dounce. The homogenate was centrifuged for 10 minutes at 800 × *g* at 4ºC, the supernatant collected, and centrifuged again using the same conditions to ensure that no unlysed cells or nuclei were present. The resulting supernatant was centrifuged for 10 minutes at 8000 × *g* at 4ºC. The supernatant was collected as the S8 cytosol; the pellet was collected as mitochondrial fraction and lysed using RIPA buffer.

Mitochondrial complex extractions and analyses. Mitochondria were isolated as described above, resuspended in extraction buffer (1M 6-amino-hexanoic acid, 50 mM Bis-Tris HCl pH 7.0), and solubilized with digitonin (final concentration 6%) on ice for 10 minutes, followed by centrifugation at 13,000 × *g* at 4ºC for 20 minutes. Glycerol (10% final concentration) and Coomassie G-250 (0.5% final concentration, only for blue native gel electrophoresis). 100 μg of sample/lane was resolved using Criterion TGX^{TM} 4-15% gels (Bio-Rad) using native conditions. For in-gel CI assays, gels were soaked in 10 ml of 5 mM Tris/HCl pH 7.4 containing NTB (25 mg) and 100 μl of 10 mg/ml NADH; for in-gel CII assays, gels were soaked in 10 ml of 5 mM Tris/HCl pH 7.4 containing NTB (25 mg), 200 μl of 1 M sodium succinate, and 8 μl of 250 mM phenazine methosulfate. All in-gel assays were performed for 30 minutes at room temperature. For CI superoxide generation measurements, CI (50 μg digitonin

extract) was stimulated with 20 μM NADH in 5 mM Tris/HCl pH 7.4; H_2O_2 production was measured using a standard AmplexRed kit (Invitrogen) supplemented with 40 U/ml human erthryocyte SOD (Sigma-Adrich) for 15 minutes at 37ºC. Following BNGE and electro-elution of CI, the same assay was performed. All assays are based on published protocols (Wittig et al., 2007; Lopez-Fabuel et al, 2016).

Metaphase chromosome spreads. Cells were seeded for 24 hours before treatment with nocodazole (50 ng/mL) for 20 hours. Floating and attached cells were collected and centrifuged at 800 × *g* for 5 minutes. Cells were resuspended in pre-warmed 75 mM KCl and incubated at 37ºC for 10 minutes with frequent inversions. Samples were centrifuged at 600 × *g* for 5 minutes, supernatants removed by inversion, and the pellets resuspended in the remaining volume of buffer. Once completely resuspended, cells were fixed by adding ice-cold fixative (3:1 ratio methanol: glacial acetic acid) in a drop-wise fashion with gentle vortexing. Samples were incubated for 10 minutes at room temperature, and then centrifuged at 1000 × *g* for 5 minutes. The fixing steps were then repeated once. The final pellet was resuspended in 0.5 mL of fixative, and dropped onto slides ensuring single drops and appropriate spreading on slides. Slides were stained with Giemsa Stain for 20 minutes, rinsed, dried, mounted with Permount Medium, and dried overnight before microscopy.

Drosophila experiments. Flies were reared on standard media at the temperatures indicated in each figure. Males and females were assessed separately. Results in the figures reflect representative experiments that have been performed independently a minimum of three times. To assess genetic modification in the eye, we recombined a *UAS MDM2* element with *GMRgal4* on the second chromosome and crossed balanced flies to control w^{1118} flies or to potential modifiers. Adult eyes of progeny were scored by eye for size, roughness, and pigmentation to assess genetic modification compared to controls and then were photographed at the same angle and magnification. For scoring, because eyes do not lie flat for quantitative measurements, we found side-by-side comparisons of populations to yield the most reliable assessment of eye phenotypes. Expressing MDM2 using *GMRgal4* substantially decreased viability at 30°C. To quantify modification of near lethality, we counted eclosed progeny and scored for balancer markers to determine which inherited the balancer and which inherited the *GMR>MDM2* chromosome for crosses to w^{1118} and each candidate modifier. Figure 2O indicates the number of progeny to eclose and the percent of each genotype expected for Mendelian

inheritance. To analyze protein expression, whole larvae were lysed in 1× RIPA buffer, and treated as indicated above.

To assess modification of wing phenotypes, we created a stock with *UAS MDM2* and *c765gal4* over the *SM6-TM6B* balancer to cross to control w^{1118} flies or to potential modifiers. Adult wings of progeny were photographed at the same magnification and then traced using ImageJ software. Flies expressing p35 and MDM2 using *c765gal4* were somewhat folded (not flat), so the reported measurements reflect only the outline of the wing, not the entire area of wing tissue and are therefore an under-estimate.

Genotypes of flies in the figures are:

w; GMRgal4/+ (Fig. 2M, 2N; labeled "Control")

w; GMRgal4, UAS MDM2/+ (Fig. 2M, 2N; labeled "MDM2")

w; GMRgal4, UAS MDM2/+; UAS DIAP1/+ (Fig. 2N)

w; GMRgal4, UAS MDM2/UAS p35 (Fig. 2N)

w; GMRgal4, UAS MDM2/+; Df(3L)H99/+ (Fig. 2N)

w; GMRgal4,UAS MDM2/ GMRgal4,UAS MDM2 (Fig. 2M; labeled "MDM2 × 2")

w; c765gal4/+ (Fig. 4T)

w; UAS ND-75^{IR}/+; c765gal4/+ (Fig. 4T)

w; UAS MDM2/+; c765gal4/+ (Fig. 4T)

w; UAS MDM2/+; c765gal4/UAS DIAP1 (Fig. S2J)

w; UAS MDM2/UAS p35; c765gal4/+ (Fig. S2J)

w; UAS MDM2/+; c765gal4/Df(3L)H99 (Fig. S2J)

Yeast transformation, growth, and expression analyses. W303 yeast were transformed with pTEF2 or pTEF-MDM2 plasmids (courtesy Barbara di Ventura, U. Heidelberg) using lithium acetate; and transformants were selected using adenine, leucine, histidine, and tryptophan on synthetic complete (SC)-glucose agar plates. For growth and expression analyses, colonies were isolated, grown in SC-glucose broth supplemented with adenine, leucine, histidine, and tryptophan. One absorbance unit (AU) at 600 nm/mL (equivalent to 1.2×10^7 cells/mL) was serially diluted 10-fold with sterile water, equal volumes of each dilution were placed on YPD and YPEG plates, incubated for 3 days at 30°C, and photographed. For protein expression analyses, yeast extracts were prepared by incubating 3.6×10^7 cells in Rodel mix (2 M NaOH, 7% 2-mercaptoethanol, 10 mM PMSF) for 10 minutes on ice; followed by dilution with 0.5 mL

water and 25% TCA (final concentration) for 10 minutes on ice. Precipitated proteins were pelleted (21,000 × *g*, 10 minutes, 4°C), washed with acetone, and air-dried. Pellets were resuspended in 1× Laemmli sample buffer, and heated at 95°C for 5 minutes. Equal volumes of yeast extracts were analyzed by SDS-PAGE and western blot with anti-MDM2 antibody (SMP14) followed by secondary antibody horseradish peroxidase conjugate (Bio-Rad, Hercules, CA, USA). Immunoblots were incubated with Super Signal West Pico Chemiluminescent Substrate and detected using a Li-Cor blot scanner.

Transgenic MDM2 mice. Transgenic MDM2 mice were obtained from Dr. Stephen N. Jones via Dr. James J. Manfredi and have been previously described (Jones et al., 1998). All animal experiments were performed in accordance with protocols approved by the Icahn School of Medicine at Mount Sinai Institutional Animal Care and Use Committee. Tail DNA and liver RNA was isolated using Qiagen DNeasy and RNeasy kits, respectively. Genotyping was performed using standard qPCR-based methods (Forward primer: 5' AGG ATC TCC TGT CAT CTC ACC TTG CTC CTG 3'; Reverse primer: 5' AAG AAC TCG TCA AGA AGG CGA TAG AAG GCG 3'). Livers were fixed in formalin, and tissues were embedded in OCT compound and frozen, or processed and embedded in paraffin, sectioned, and stained as indicated. Whole cell lysates were generated by homogenizing 100 mg of tissue in MIB, adding an equal volume of RIPA buffer, incubating on ice for 20 minutes, and insoluble material was pelleted (21,000 × *g*, 10 minutes, 4°C). Mitochondria were isolated as indicated above, and subjected to BNGE, CI assays, and superoxide generation measurements.

SUPPLEMENTAL INFORMATION AND LEGENDS

Figure S1. Experiments related to figure 1.

(A) Whole cell lysates from H1299 stably expressing *MDMX* RNAi were analyzed by SDS-PAGE and western blot for indicated proteins. β-Actin is the loading control.

(B - C) H1299 were transfected with pcDNA.MDMX (0, 0.1, 0.2, 0.4, 0.8 μg) for 24 hours in the presence of zVAD-fmk (100 μM); total RNA and protein were analyzed by qPCR and western blot for MDMX expression. CT are untreated cells. The DNA mass was scaled for western blot detection of protein, and reduced for 96 well format IncuCyte experiments.

(D - F) H1299 were transfected with indicated MDM2, MDMX, and p53 plasmids, and the kinetics of cell death were detected using an IncuCyte Zoom.

Figure S2. Experiments related to figure 2.

(A - B) H1299 stably expressing *BIM* or *BAX* RNAi were generated. Total RNA and protein were analyzed by qPCR and western blot for *BIM (A)* and *BAX (B)* knock-down efficiency, respectively.

(C) H1299 were transfected with pcDNA.MDM2^{WT} (0.5 μg), and CHAPS lysates were subjected to immunoprecipitation with the anti-BAX clone 6A7. Total cell lysates were also analyzed by SDS-PAGE and western blot for indicated proteins. β-Actin is the loading control.

(D - E) H1299 stably expressing *BAK*, *BID*, or *PUMA* RNAi were generated. Total RNA and protein were analyzed by qPCR *(D)* and western blot *(E)* for knock-down efficiency, respectively.

(F - G) Indicated control (pLKO) and stable RNAi lines from *D-E* were transfected with pcDNA.MDM2 *(F)* or pcDNA.control *(G)* and the kinetics of cell death were detected using an IncuCyte Zoom.

(H) Whole larval lysates were analyzed by SDS-PAGE and western blot for indicated proteins to confirm MDM2 expression.

(I) Representative images of *Drosophila* expressing transgenic *MDM2* under control of the eye-specific *GMR* promoter (*GMR>MDM2*). The *Gal4/UAS* system is temperature sensitive, and animals were reared at indicated temperatures to increase MDM2 levels. Images shown are female eyes. Fly from 30°C is a dissected pharate adult.

(J) Representative images of *Drosophila* expressing transgenic *MDM2* under control of the wing-specific *GMR* promoter (*c765>MDM2*) with *H99* deletion, or co-expressing *DIAP1* or *p35*. "*c765gal4/+*" is the control wing. Studies were performed at 21°C.

Figure S3. Experiments related to figure 4.

(A) H1299 were untreated (Control), mock transfected (No DNA transfection but Lipofectamine2000), or transfected with empty pCMV (0.25 μg), cultured for 24 hours, and subjected to Seahorse XF Cell Mito Stress analysis.

(B) Whole cell lysates from U-2OS and SJSA-1 cells were analyzed by SDS-PAGE and western blot for indicated proteins.

(C - D) U-2 OS were treated with Nutlin-3A (1 μM) for 48 hours, and subjected to Seahorse XF Cell Mito Stress analysis. A representative MitoStress assay *(C)* and endpoint data are shown *(D)*.

(E - G) U-2 OS and SJSA-1 were treated with Nutlin-3A (1 μM) for indicated times. Total RNA and protein were analyzed by qPCR *(E-F)* and western blot *(G)* for MDM2 induction.

Figure S4. Additional experiments related to figure 4.

(A) 20 ng of GST-MDM2^{WT} was loaded with endogenous NDUFS1 in PBS, captured on Protein A beads containing anti-MDM2 (clone SMP14), and incubated in the presence of 6HIS-p53 (10, 25, 50 ng) for 1 hour at RT before washing and analyses via SDS-PAGE and western blot for indicated proteins. GST-MDM2 + p53 (no NDUFS1) demonstrates maximal binding. V_H and V_L are the heavy and light chains from the SMP14 antibody, respectively.

(B) SDS-PAGE and Coomassie Blue Staining of GST-MDM2^{WT} and GST-MDM2^{C464A} protein fractions following GSH-Sepharose chromatography. Indicated fractions (white hatched box) were combined and utilized.

(C) Combined fractions from *B* were analyzed by SDS-PAGE and western blot.

(D) H1299 were transfected with pCMV-MDM2^{WT} or pCMV-MDM2^{C464A} (1 μg each) for 24 hours in the presence of zVAD-fmk (100 μM), cytosolic extracts were subjected to anti-MDM2 immunoprecipitation, and complexes were analyzed by western blot for indicated proteins.

(E) H1299 were transfected with indicated MDM2 mutants (1 μg each), cultured for 24 hours in the presence of zVAD-fmk (100 μM), and cytosolic extracts were subjected to anti-MDM2

immunoprecipitation, and complexes were analyzed by western blot for indicated proteins. Whole cell lysates were also analyzed to ensure NDUFS1 was equally expressed in all transfections.

(F) H1299 were transfected with indicated pCMV MDM2 variants (0.25 μg) in the presence of zVAD-fmk (100 μM), cultured for 24 hours, fixed, and stained for MDM2 localization. Scale bar = 10 μm.

(G) H1299 were transfected with pCMV-MDM2^{WT} or pCMV-MDM2^{G58I} (1 μg each) for 24 hours in the presence of zVAD-fmk (100 μM). Cytosolic, mitochondrial, and total cell lysates were analyzed by SDS-PAGE and western blot for indicated proteins.

Figure

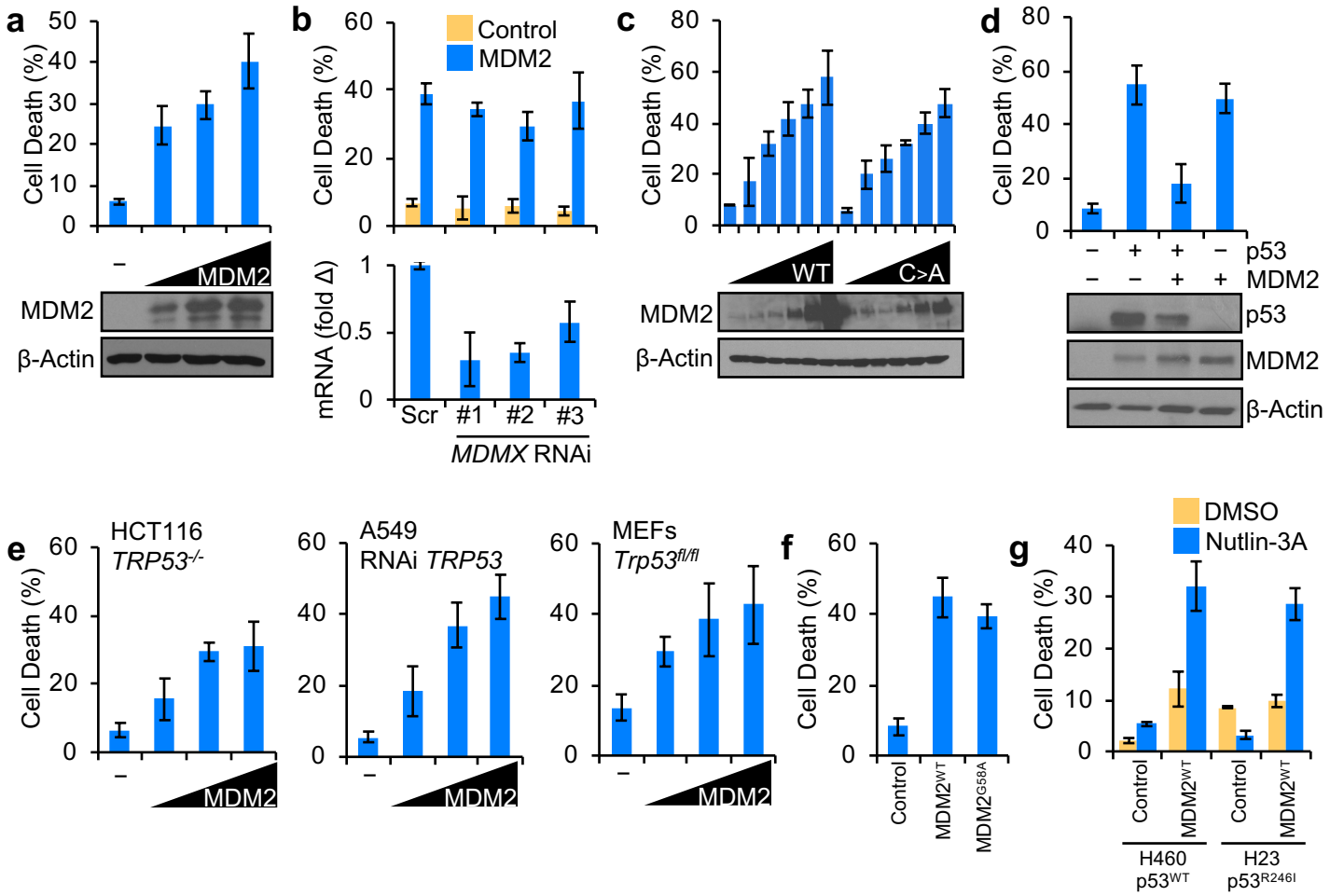
a
Cell Death (%)
MDM2
β-Actin
b
Control
MDM2
Cell Death (%)
mRNA (fold Δ)
Scr
#1
#2
#3
MDMX RNAi
c
Cell Death (%)
WT
C>A
MDM2
β-Actin
d
Cell Death (%)
p53
MDM2
β-Actin

e
HCT116
TRP53-/-
A549
RNAi TRP53
MEFs
Trp53fl/fl
Cell Death (%)
MDM2
f
Cell Death (%)
Control
MDM2WT
MDM2G58A
g
DMSO
Nutlin-3A
Cell Death (%)
Control
MDM2WT
H460
p53WT
H23
p53R246I

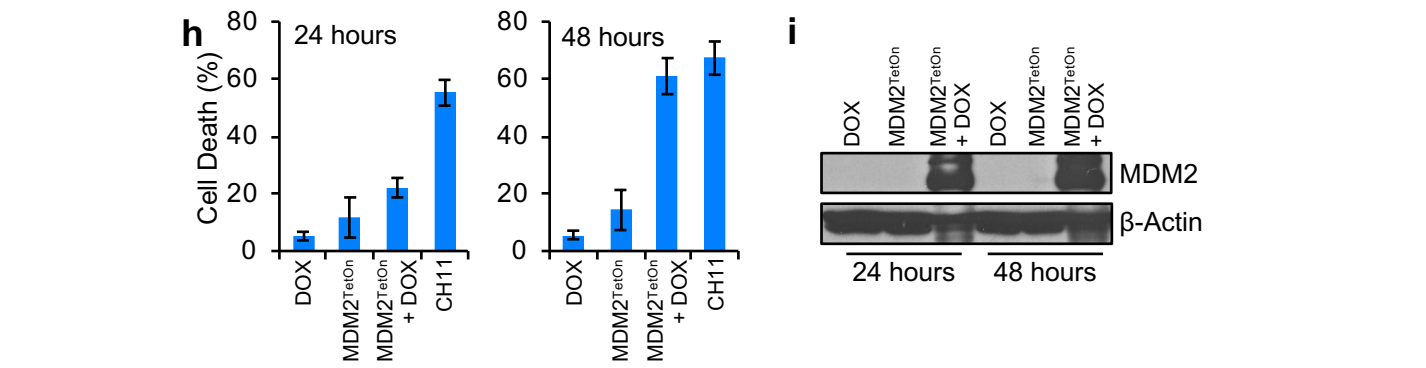
h
24 hours
48 hours
Cell Death (%)
DOX
MDM2TetOn
MDM2TetOn + DOX
CH11
i
DOX
MDM2TetOn
MDM2TetOn + DOX
MDM2
β-Actin
24 hours
48 hours

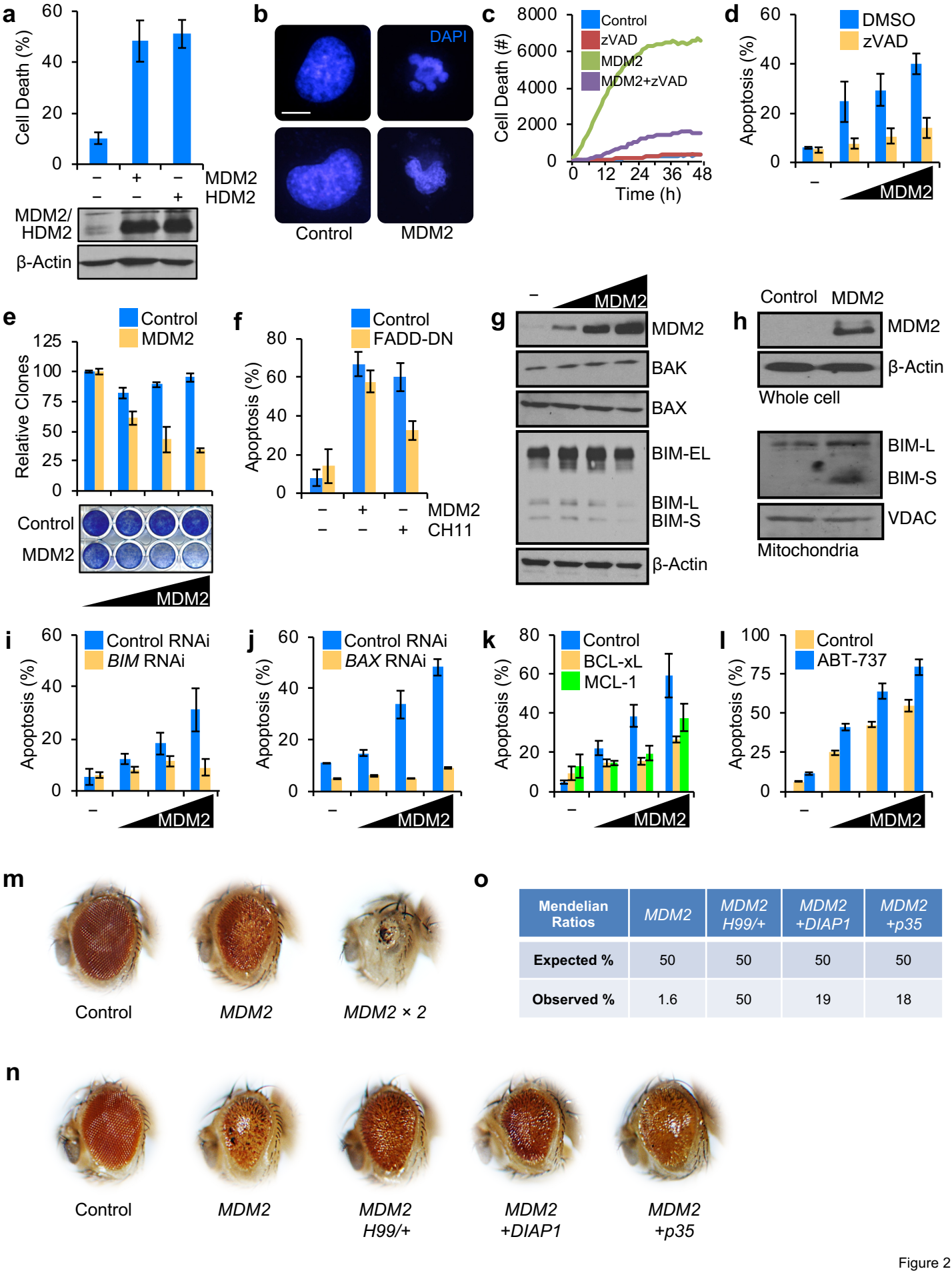

m

o

Mendelian Ratios	*MDM2*	*MDM2 H99/+*	*MDM2 +DIAP1*	*MDM2 +p35*
Expected %	50	50	50	50
Observed %	1.6	50	19	18

n

Figure 2

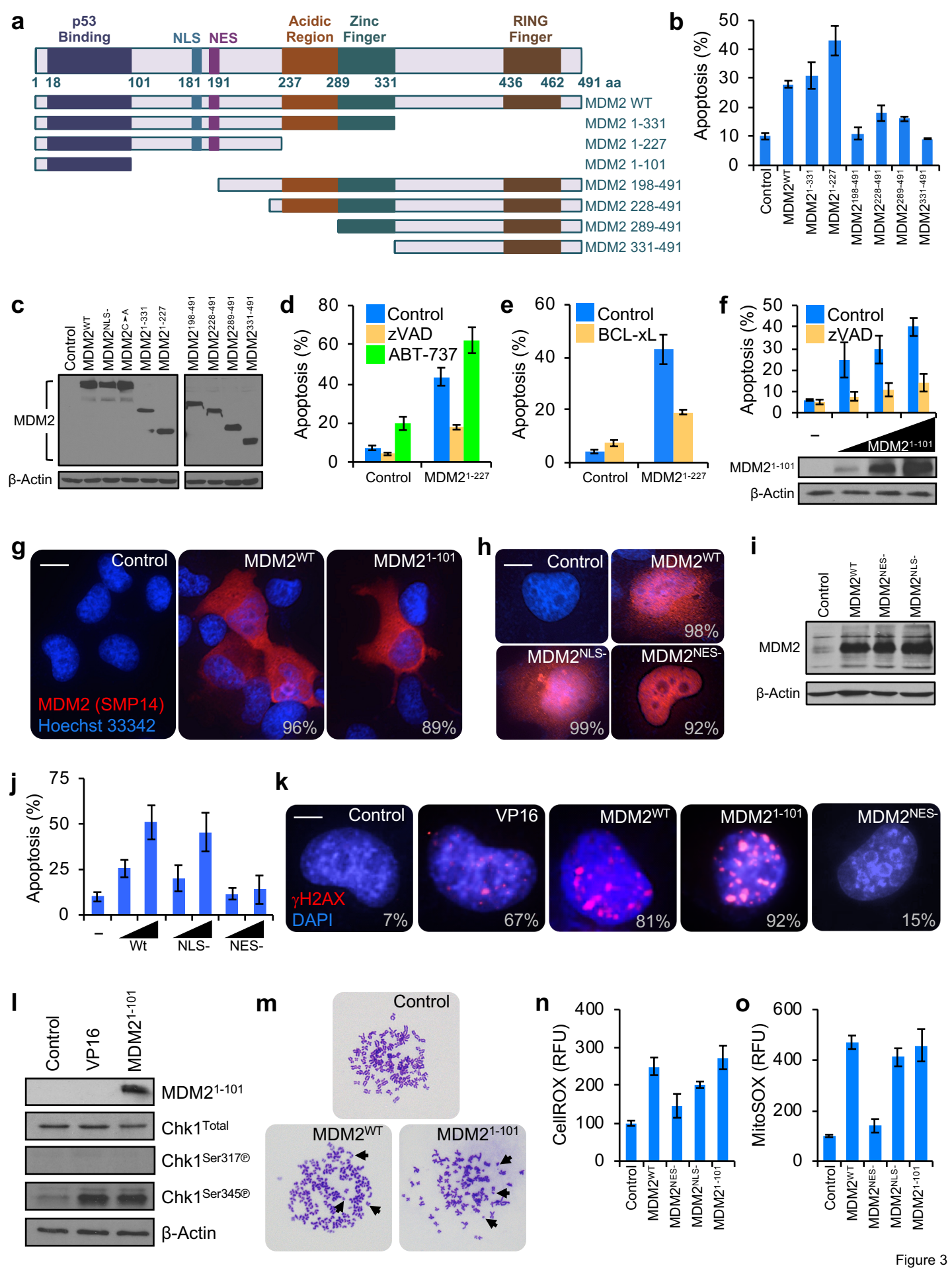
a
p53 Binding
NLS
NES
Acidic Region
Zinc Finger
RING Finger
1 18 101 181 191 237 289 331 436 462 491 aa
MDM2 WT
MDM2 1-331
MDM2 1-227
MDM2 1-101
MDM2 198-491
MDM2 228-491
MDM2 289-491
MDM2 331-491
b
Apoptosis (%)
Control
MDM2WT
MDM2NLS-
MDM2C➤A
MDM2 1-331
MDM2 1-227
MDM2 198-491
MDM2 228-491
MDM2 289-491
MDM2 331-491
c
MDM2
β-Actin
d
Control
zVAD
ABT-737
Apoptosis (%)
Control
MDM2 1-227
e
Control
BCL-xL
Apoptosis (%)
Control
MDM2 1-227
f
Control
zVAD
Apoptosis (%)
MDM2 1-101
MDM2 1-101
β-Actin
g
Control
MDM2WT
MDM2 1-101
MDM2 (SMP14)
Hoechst 33342
96%
89%
h
Control
MDM2WT
98%
MDM2NLS-
MDM2NES-
99%
92%
i
Control
MDM2WT
MDM2NES-
MDM2NLS-
MDM2
β-Actin
j
Apoptosis (%)
–
Wt
NLS-
NES-
k
Control
VP16
MDM2WT
MDM2 1-101
MDM2NES-
γH2AX
DAPI
7%
67%
81%
92%
15%
l
Control
VP16
MDM2 1-101
MDM2 1-101
Chk1 Total
Chk1 Ser317P
Chk1 Ser345P
β-Actin
m
Control
MDM2WT
MDM2 1-101
n
CellROX (RFU)
Control
MDM2WT
MDM2NES-
MDM2NLS-
MDM2 1-101
o
MitoSOX (RFU)
Control
MDM2WT
MDM2NES-
MDM2NLS-
MDM2 1-101

Figure 3

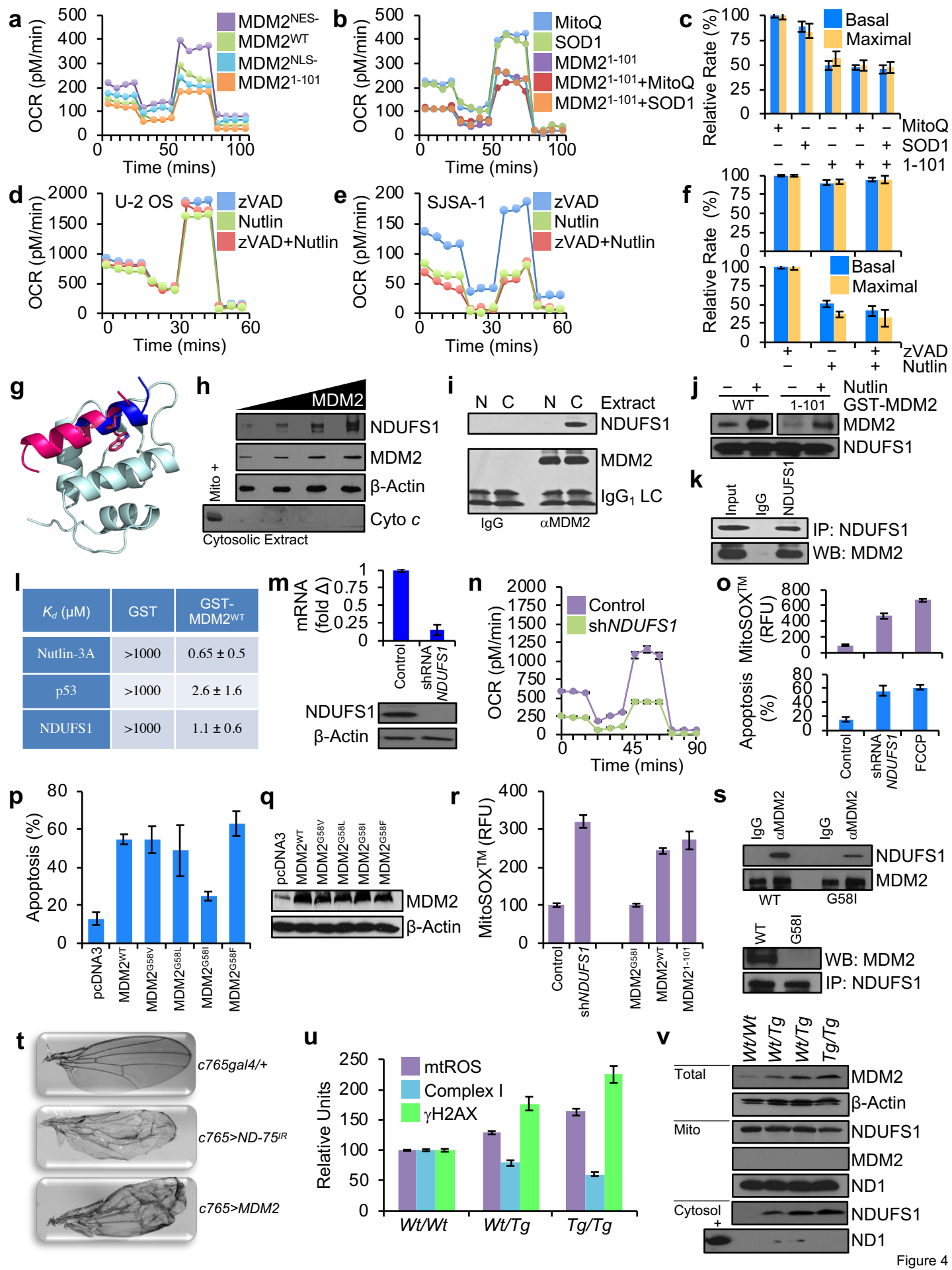
a
OCR (pM/min)
Time (mins)
MDM2NES-
MDM2WT
MDM2NLS-
MDM21-101
b
MitoQ
SOD1
MDM21-101
MDM21-101+MitoQ
MDM21-101+SOD1
c
Relative Rate (%)
Basal
Maximal
MitoQ
SOD1
1-101
d
U-2 OS
zVAD
Nutlin
zVAD+Nutlin
e
SJSA-1
f
zVAD
Nutlin
g
h
MDM2
NDUFS1
MDM2
β-Actin
Cyto c
Mito +
Cytosolic Extract
i
N C N C
Extract
NDUFS1
MDM2
IgG1 LC
IgG
αMDM2
j
Nutlin
GST-MDM2
WT
1-101
MDM2
NDUFS1
k
Input
IgG
NDUFS1
IP: NDUFS1
WB: MDM2
l
Kd (μM)
GST
GST-MDM2WT
Nutlin-3A
>1000
0.65 ± 0.5
p53
>1000
2.6 ± 1.6
NDUFS1
>1000
1.1 ± 0.6
m
mRNA (fold Δ)
Control
shRNA NDUFS1
NDUFS1
β-Actin
n
Control
shNDUFS1
Time (mins)
o
MitoSOX™ (RFU)
Apoptosis (%)
Control
shRNA NDUFS1
FCCP
p
Apoptosis (%)
pcDNA3
MDM2WT
MDM2G58V
MDM2G58L
MDM2G58I
MDM2G58F
q
MDM2
β-Actin
r
MitoSOX™ (RFU)
Control
shNDUFS1
MDM2G58I
MDM2WT
MDM21-101
s
IgG
αMDM2
NDUFS1
MDM2
WT
G58I
WB: MDM2
IP: NDUFS1
t
c765gal4/+
c765>ND-75IR
c765>MDM2
u
Relative Units
mtROS
Complex I
γH2AX
Wt/Wt
Wt/Tg
Tg/Tg
v
Wt/Wt
Wt/Tg
Wt/Tg
Tg/Tg
Total
Mito
Cytosol
MDM2
β-Actin
NDUFS1
MDM2
ND1
NDUFS1
ND1

Figure 4

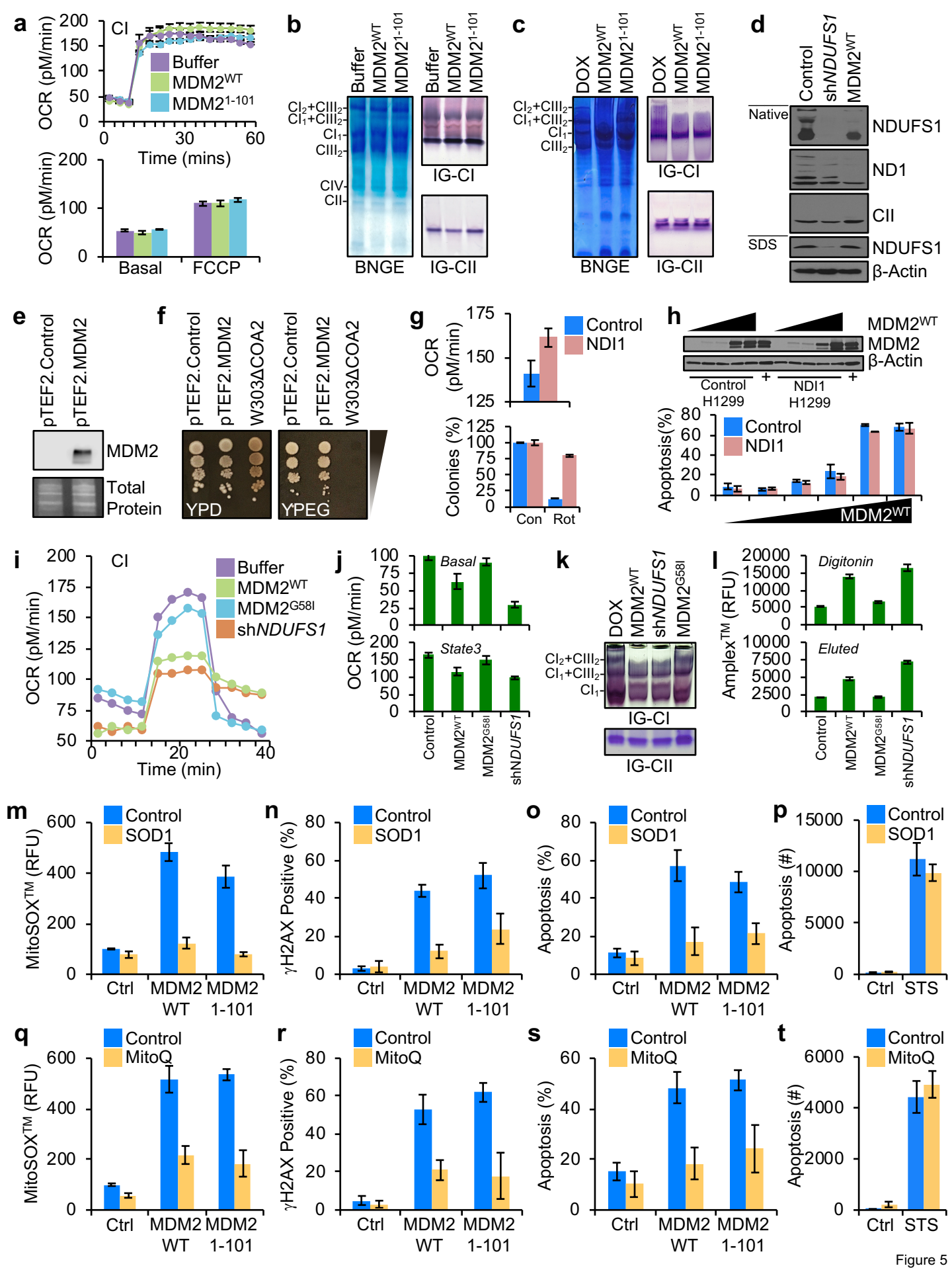
a
CI
OCR (pM/min)
Buffer
MDM2WT
MDM2 1-101
Time (mins)
Basal
FCCP
b
Buffer
MDM2WT
MDM2 1-101
CI2+CIII2
CI1+CIII2
CI1
CIII2
CIV
CII
BNGE
IG-CI
IG-CII
c
DOX
MDM2WT
MDM2 1-101
BNGE
IG-CI
IG-CII
d
Control
shNDUFS1
MDM2WT
Native
NDUFS1
ND1
CII
SDS
NDUFS1
β-Actin
e
pTEF2.Control
pTEF2.MDM2
MDM2
Total Protein
f
pTEF2.Control
pTEF2.MDM2
W303ΔCOA2
YPD
YPEG
g
OCR (pM/min)
Control
NDI1
Colonies (%)
Con
Rot
h
MDM2WT
MDM2
β-Actin
Control H1299
NDI1 H1299
Apoptosis(%)
Control
NDI1
MDM2WT
i
CI
OCR (pM/min)
Buffer
MDM2WT
MDM2G58I
shNDUFS1
Time (min)
j
Basal
State3
OCR (pM/min)
Control
MDM2WT
MDM2G58I
shNDUFS1
k
DOX
MDM2WT
shNDUFS1
MDM2G58I
CI2+CIII2
CI1+CIII2
CI1
IG-CI
IG-CII
l
Digitonin
Eluted
Amplex™ (RFU)
Control
MDM2WT
MDM2G58I
shNDUFS1
m
Control
SOD1
MitoSOX™ (RFU)
Ctrl
MDM2 WT
MDM2 1-101
n
Control
SOD1
γH2AX Positive (%)
Ctrl
MDM2 WT
MDM2 1-101
o
Control
SOD1
Apoptosis (%)
Ctrl
MDM2 WT
MDM2 1-101
p
Control
SOD1
Apoptosis (#)
Ctrl
STS
q
Control
MitoQ
MitoSOX™ (RFU)
Ctrl
MDM2 WT
MDM2 1-101
r
Control
MitoQ
γH2AX Positive (%)
Ctrl
MDM2 WT
MDM2 1-101
s
Control
MitoQ
Apoptosis (%)
Ctrl
MDM2 WT
MDM2 1-101
t
Control
MitoQ
Apoptosis (#)
Ctrl
STS

Figure 5

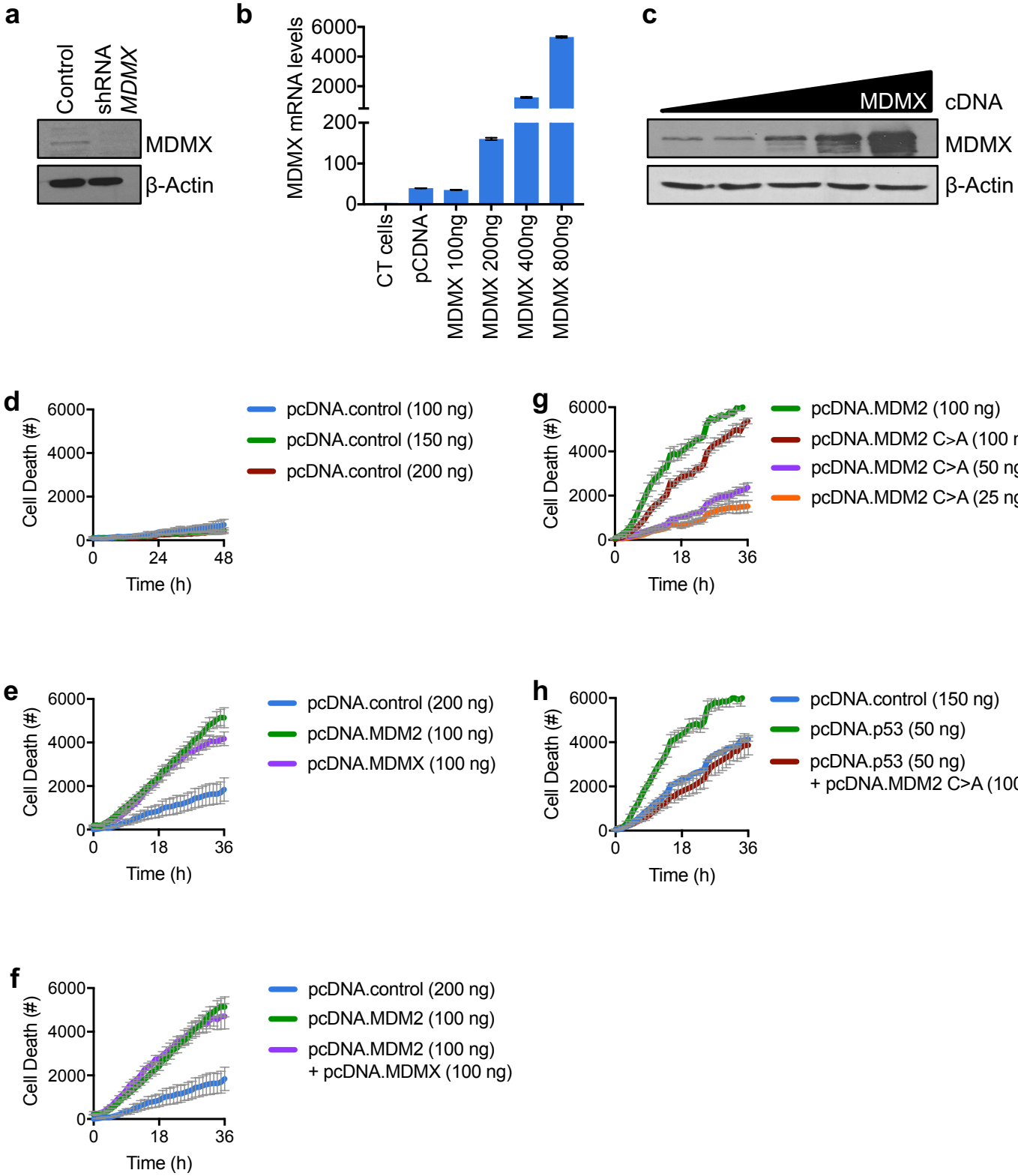
a
Control
shRNA
MDMX
MDMX
β-Actin
b
MDMX mRNA levels
6000
4000
2000
200
100
0
CT cells
pCDNA
MDMX 100ng
MDMX 200ng
MDMX 400ng
MDMX 800ng
c
MDMX
cDNA
MDMX
β-Actin
d
Cell Death (#)
6000
4000
2000
0
0
24
48
Time (h)
pcDNA.control (100 ng)
pcDNA.control (150 ng)
pcDNA.control (200 ng)
g
Cell Death (#)
6000
4000
2000
0
0
18
36
Time (h)
pcDNA.MDM2 (100 ng)
pcDNA.MDM2 C>A (100 ng)
pcDNA.MDM2 C>A (50 ng)
pcDNA.MDM2 C>A (25 ng)
e
Cell Death (#)
6000
4000
2000
0
0
18
36
Time (h)
pcDNA.control (200 ng)
pcDNA.MDM2 (100 ng)
pcDNA.MDMX (100 ng)
h
Cell Death (#)
6000
4000
2000
0
0
18
36
Time (h)
pcDNA.control (150 ng)
pcDNA.p53 (50 ng)
pcDNA.p53 (50 ng)
+ pcDNA.MDM2 C>A (100 ng)
f
Cell Death (#)
6000
4000
2000
0
0
18
36
Time (h)
pcDNA.control (200 ng)
pcDNA.MDM2 (100 ng)
pcDNA.MDM2 (100 ng)
+ pcDNA.MDMX (100 ng)

Figure S1

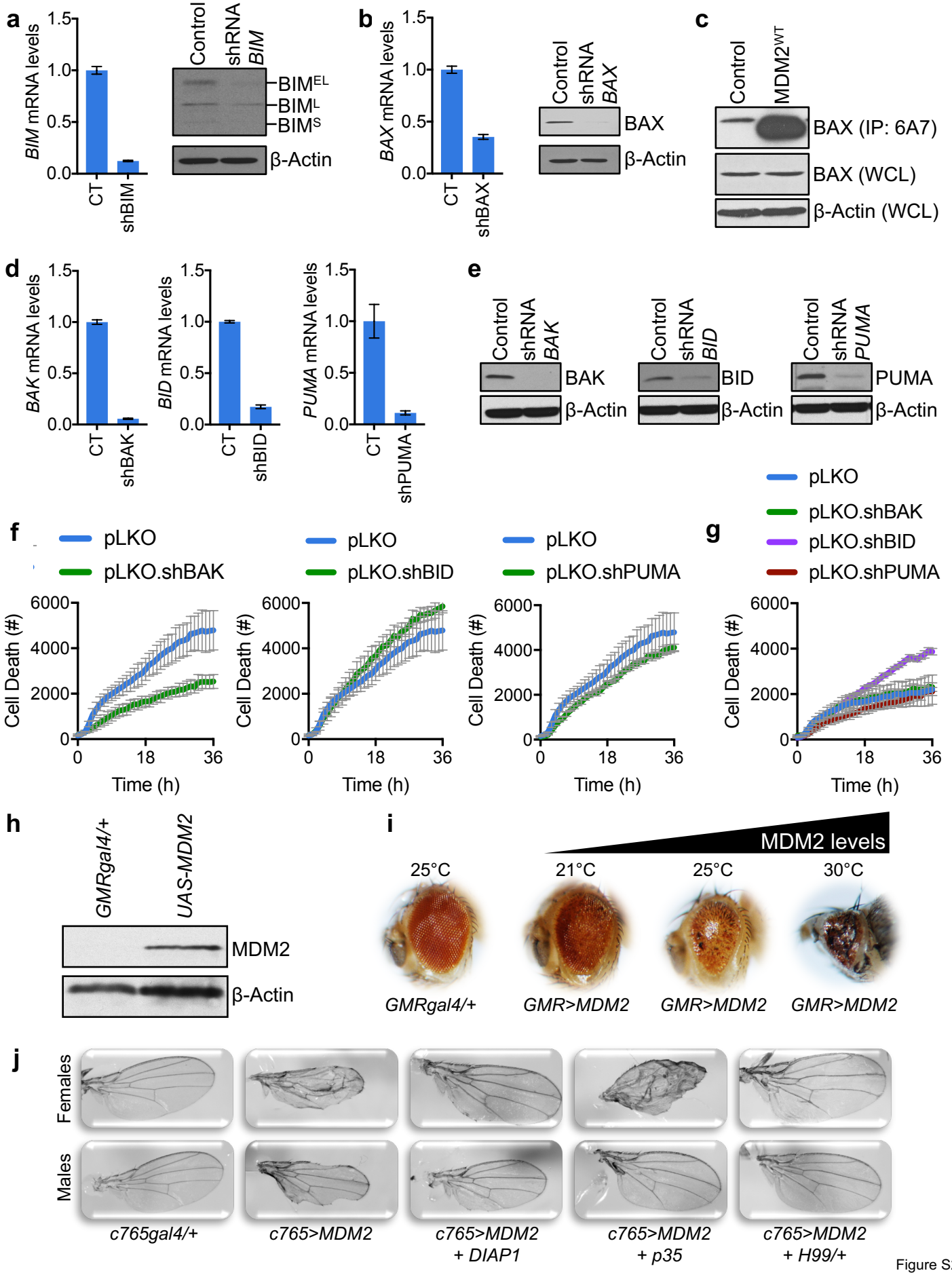
a
BIM mRNA levels
1.5
1.0
0.5
0.0
CT
shBIM
Control
shRNA BIM
BIM^EL
BIM^L
BIM^S
β-Actin
b
BAX mRNA levels
CT
shBAX
Control
shRNA BAX
BAX
β-Actin
c
Control
MDM2^WT
BAX (IP: 6A7)
BAX (WCL)
β-Actin (WCL)
d
BAK mRNA levels
shBAK
BID mRNA levels
shBID
PUMA mRNA levels
shPUMA
e
Control
shRNA BAK
BAK
β-Actin
shRNA BID
BID
shRNA PUMA
PUMA
f
pLKO
pLKO.shBAK
pLKO.shBID
pLKO.shPUMA
Cell Death (#)
6000
4000
2000
0
18
36
Time (h)
g
pLKO
pLKO.shBAK
pLKO.shBID
pLKO.shPUMA
h
GMRgal4/+
UAS-MDM2
MDM2
β-Actin
i
MDM2 levels
25°C
21°C
25°C
30°C
GMRgal4/+
GMR>MDM2
GMR>MDM2
GMR>MDM2
j
Females
Males
c765gal4/+
c765>MDM2
c765>MDM2 + DIAP1
c765>MDM2 + p35
c765>MDM2 + H99/+

Figure S2

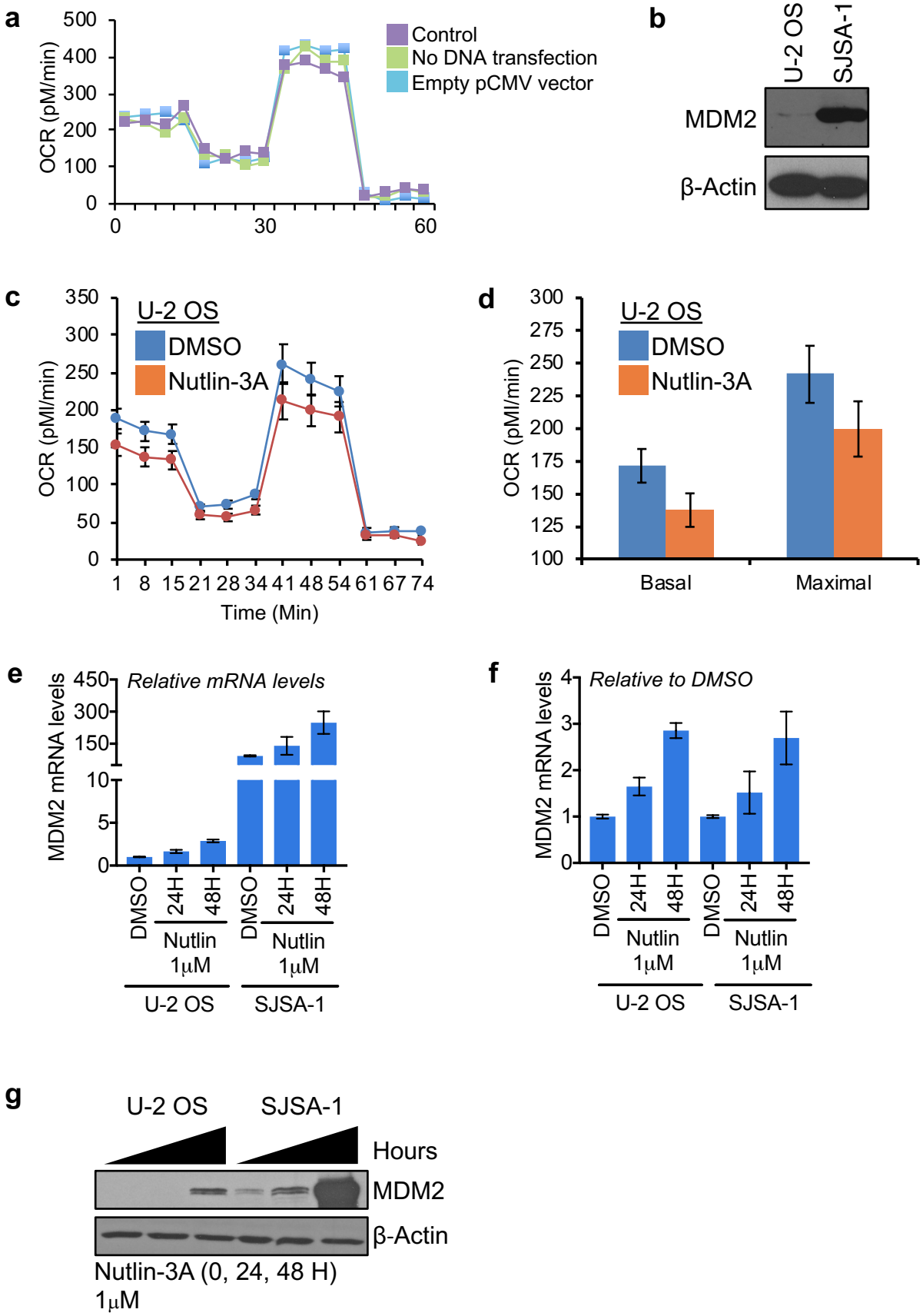
a
OCR (pM/min)
500
400
300
200
100
0
0
30
60
Control
No DNA transfection
Empty pCMV vector
b
U-2 OS
SJSA-1
MDM2
β-Actin
c
U-2 OS
DMSO
Nutlin-3A
OCR (pMl/min)
350
300
250
200
150
100
50
0
1 8 15 21 28 34 41 48 54 61 67 74
Time (Min)
d
U-2 OS
DMSO
Nutlin-3A
OCR (pMl/min)
300
275
250
225
200
175
150
125
100
Basal
Maximal
e
Relative mRNA levels
MDM2 mRNA levels
450
300
150
10
5
0
DMSO
24H
48H
DMSO
24H
48H
Nutlin 1μM
Nutlin 1μM
U-2 OS
SJSA-1
f
Relative to DMSO
MDM2 mRNA levels
4
3
2
1
0
DMSO
24H
48H
DMSO
24H
48H
Nutlin 1μM
Nutlin 1μM
U-2 OS
SJSA-1
g
U-2 OS
SJSA-1
Hours
MDM2
β-Actin
Nutlin-3A (0, 24, 48 H)
1μM

Figure S3

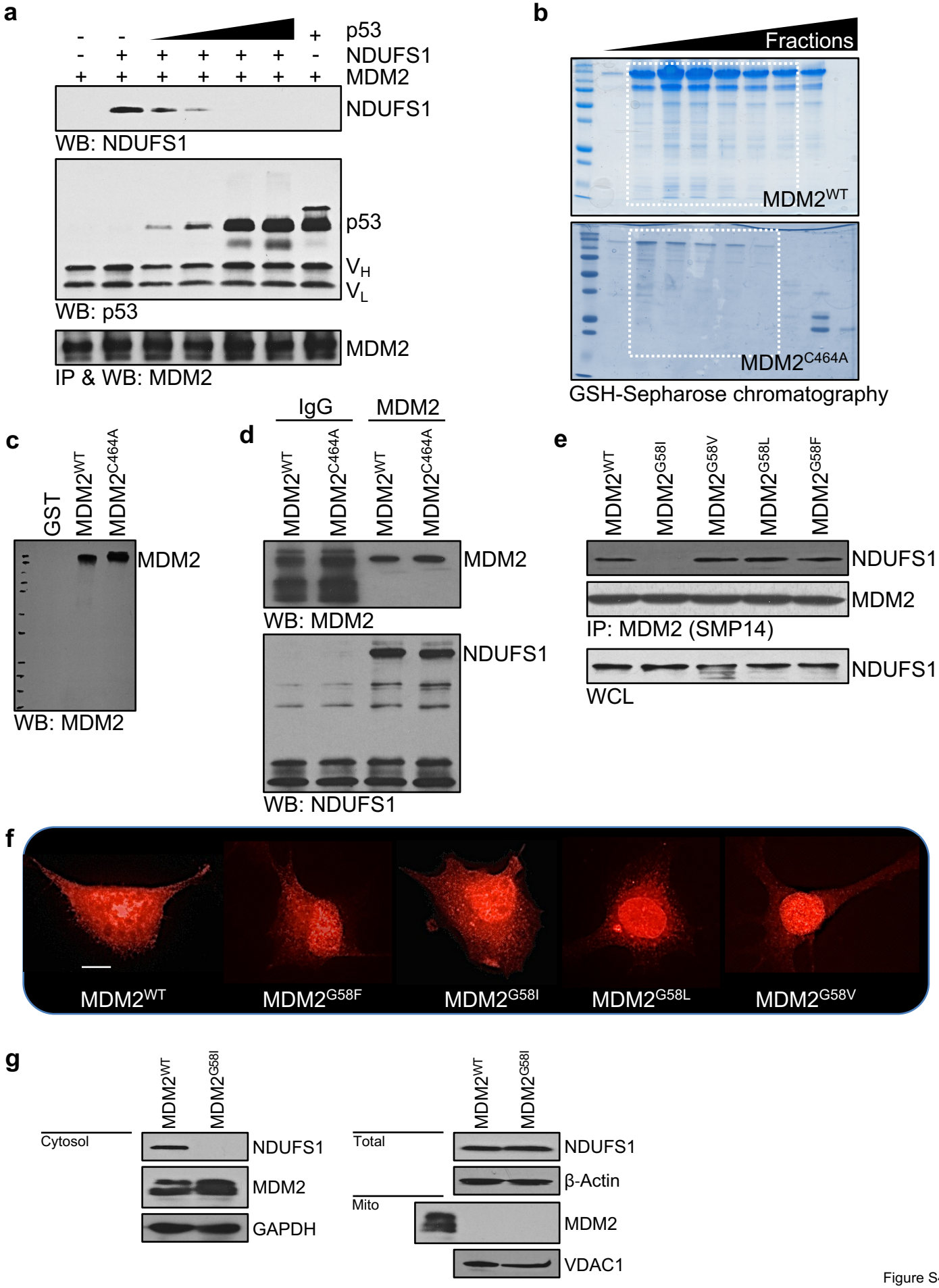
a
p53
NDUFS1
MDM2
NDUFS1
WB: NDUFS1
p53
V_H
V_L
WB: p53
MDM2
IP & WB: MDM2
b
Fractions
$MDM2^{WT}$
$MDM2^{C464A}$
GSH-Sepharose chromatography
c
GST
$MDM2^{WT}$
$MDM2^{C464A}$
MDM2
WB: MDM2
d
IgG
MDM2
$MDM2^{WT}$
$MDM2^{C464A}$
$MDM2^{WT}$
$MDM2^{C464A}$
MDM2
WB: MDM2
NDUFS1
WB: NDUFS1
e
$MDM2^{WT}$
$MDM2^{G58I}$
$MDM2^{G58V}$
$MDM2^{G58L}$
$MDM2^{G58F}$
NDUFS1
MDM2
IP: MDM2 (SMP14)
NDUFS1
WCL
f
$MDM2^{WT}$
$MDM2^{G58F}$
$MDM2^{G58I}$
$MDM2^{G58L}$
$MDM2^{G58V}$
g
$MDM2^{WT}$
$MDM2^{G58I}$
Cytosol
NDUFS1
MDM2
GAPDH
$MDM2^{WT}$
$MDM2^{G58I}$
Total
NDUFS1
β-Actin
Mito
MDM2
VDAC1

Figure S4